

₁ Study of neutrino-nucleus interaction at around 1 GeV using
₂ a 3D grid-structure neutrino detector, WAGASCI, muon
₃ range detectors and magnetized spectrometer, Baby MIND,
₄ at J-PARC neutrino monitor hall

₅ A. Bonnemaison, R. Cornat, L. Domine, O. Drapier, O. Ferreira, F. Gastaldi,
₆ M. Gonin, J. Imber, M. Licciardi, F. Magniette, T. Mueller, L. Vignoli, and O. Volcy
₇ *Ecole Polytechnique, IN2P3-CNRS, Laboratoire Leprince-Ringuet, Palaiseau,*
₈ *France*

₉ S. Cao and T. Kobayashi

₁₀ *High Energy Accelerator Research Organization (KEK), Tsukuba, Ibaraki, Japan*

₁₁ M. Khabibullin, A. Khotjantsev, A. Kostin, Y. Kudenko, A. Mefodiev, O. Mineev,
₁₂ S. Suvorov, and N. Yershov

₁₃ *Institute for Nuclear Research of the Russian Academy of Sciences, Moscow, Russia*

₁₄ B. Quilain

₁₅ *Kavli Institute for the Physics and Mathematics of the Universe (WPI), The*
₁₆ *University of Tokyo Institutes for Advanced Study, University of Tokyo, Kashiwa,*
₁₇ *Chiba, Japan*

₁₈ T. Hayashino, A. Hiramoto, A.K. Ichikawa, K. Nakamura, T. Nakaya, K Yasutome,
₁₉ and K. Yoshida

₂₀ *Kyoto University, Department of Physics, Kyoto, Japan*

₂₁ Y. Azuma, J. Harada, T. Inoue, K. Kin, N. Kukita, S. Tanaka, Y. Seiya,
₂₂ K. Wakamatsu, and K. Yamamoto

₂₃ *Osaka City University, Department of Physics, Osaka, Japan*

24 A. Blondel, F. Cadoux, Y. Favere, E. Noah, L. Nicola, and S. Parsa

25 *University of Geneva, Section de Physique, DPNC, Geneva, Switzerland*

26 N. Chikuma, F. Hosomi, T. Koga, R. Tamura, and M. Yokoyama

27 *University of Tokyo, Department of Physics, Tokyo, Japan*

28 Y. Hayato

29 *University of Tokyo, Institute for Cosmic Ray Research, Kamioka Observatory,*
30 *Kamioka, Japan*

31 Y. Asada, K. Matsushita, A. Minamino, K. Okamoto, and D. Yamaguchi

32 *Yokohama National University, Faculty of Engineering, Yokohama, Japan*

33 December 14, 2017

34 **Contents**

35	1	Introduction	3
36	2	Experimental Setup	4
37	2.1	Wagasci modules	5
38	2.1.1	Detector	5
39	2.1.2	Electronics	8
40	2.1.3	Water system	9
41	2.2	INGRID Proton module	10
42	2.3	Baby MIND	11
43	2.3.1	Magnet modules	11
44	2.3.2	Scintillator modules	12
45	2.3.3	Electronics	14
46	2.3.4	Pefromance check	15
47	2.4	Side muon range detector	16

48	3 Physics goals	18
49	3.1 Expected number of events	19
50	3.2 Pseudo-monochromatic beam by using different off-axis fluxes	19
51	3.3 Subjects Wagasci can contribute	21
52	4 Status of J-PARC T59 experiment	22
53	5 MC studies	23
54	5.1 Detector simulation	23
55	5.1.1 Detector geometry	24
56	5.1.2 Response of detector components	25
57	5.2 Track reconstruction	25
58	5.3 Event selection	25
59	5.4 Cross section measurements	29
60	6 Standalone WAGASCI-module performances	31
61	6.1 Reconstruction algorithm	33
62	6.1.1 Description	33
63	6.1.2 Performances	35
64	6.2 Background subtraction: the water-out module	41
65	7 Schedule	44
66	8 Requests	44
67	8.1 Neutrino beam	44
68	8.2 Equipment request including power line	44
69	8.2.1 Baby MIND Equipment request including power line	45
70	9 Conclusion	45

71 **1 Introduction**

72 The understanding of neutrino-nucleus interactions in the 1 GeV energy region is critical
 73 for the success of accelerator-based neutrino oscillation experiments such as the T2K exper-
 74 iment. Complicated multi-body effects of nuclei render this understanding difficult. The
 75 T2K near detectors have been measuring these and significant progress has been achieved.
 76 However, the understanding is still limited. One of the big factors preventing from full
 77 understanding is the non-monochromatic neutrino beam spectrum. Measurements with
 78 different but some overlapping beam spectra would greatly benefit to resolve the contrib-
 79 ution from different neutrino energies. We, the Wagasci collaboration, proposes to study
 80 the neutrino-nucleus interaction at the B2 floor of the neutrino monitor building, where

81 different neutrino spectra can be obtained due to the different off-axis position. Our exper-
82 imental setup contains 3D grid-structure plastic-scintillator detectors filled with water as
83 the neutrino interaction target (Wagasci modules), two side- and one downstream- muon
84 range detectors(MRD's). The 3D grid-structure and side-MRD's allows a measurement of
85 wider-angle scattering than the T2K off-axis near detector (ND280). High water to scintil-
86 lator material ratio enables the measurement of the neutrino interaction on water, which
87 is highly desired for the T2K experiment because it's far detector, Super-Kamiokande,
88 is composed of water. The MRD's consist of plastic scintillators and iron plates. The
89 downstream-MRD, so called the Baby MIND detector, also works as a magnet and pro-
90 vides the charge identification capability as well as magnetic momentum measurement for
91 high energy muons. The charge identification is essentially important to select antineu-
92 trino events in the antineutrino beam because contamination of the neutrino events is as
93 high as 30%. Most of the detectors has been already constructed. The Wagasci modules
94 have been commissioned as the J-PARC T59 experiment and the Baby MIND detector was
95 commissioned at the CERN neutrino platform. Therefore, the collaboration will be ready
96 to proceed to the physics data taking for the T2K beam time in January 2019. We will
97 provide the cross sections of the charged current neutrino and antineutrino interactions on
98 water with slightly higher neutrino energy than T2K ND280 with wide angler acceptance.
99 When combined with ND280 measurements, our measurement would greatly improve the
100 understanding of the neutrino interaction at around 1 GeV and contribute to reduce one
101 of the most significant uncertainty of the T2K experiment.

102 **2 Experimental Setup**

103 Figure. 1 and 2 show a schematic view and a CAD drawing of the entire set of detectors.
104 Central neutrino target detectors consist of two Wagasci modules and T2K INGRID proton
105 module. Inside the Wagasci module, plastic scintillator bars are aligned as a 3D grid-like
106 structure and spaces in the structure are filled with water for a water-in Wagasci module.
107 T2K INGRID proton module is a full active neutrino target detector which is composed
108 only with scintillator bars in its tracking region. The central detectors are surrounded by
109 two side- and one downstream- muon range detectors(MRD's) The MRD's are used to select
110 muon tracks from the charged-current (CC) interactions and to reject short tracks caused by
111 neutral particles that originate mainly from neutrino interactions in material surrounding
112 the central detector, like the walls of the detector hall, neutrons and gammas, or neutral-
113 current (NC) interactions. The muon momentum can be reconstructed from its range
114 inside the detector. The MRD's consist of plastic scintillators and iron plates. In addition,
115 each of the iron plates of the downstream-MRD, so called the Baby MIND detector, is
116 wound by a coil and can be magnetized. It provide the charge selection capability.

117 For all detectors, scintillation light in the scintillator bar is collected and transported
118 to a photodetector with a wavelength shifting fiber (WLS fiber). The light is read out by

119 a photodetector, Multi-Pixel Photon Counter (MPPC), attached to one end of the WLS
120 fiber. The signal from the MPPC is read out by the dedicated electronics developed for the
121 test experiment to enable bunch separation in the beam spill. The readout electronics is
122 triggered using the beam-timing signal from MR to synchronize to the beam. The beam-
123 timing signal is branched from those for T2K, and will not cause any effect on the T2K
124 data taking.

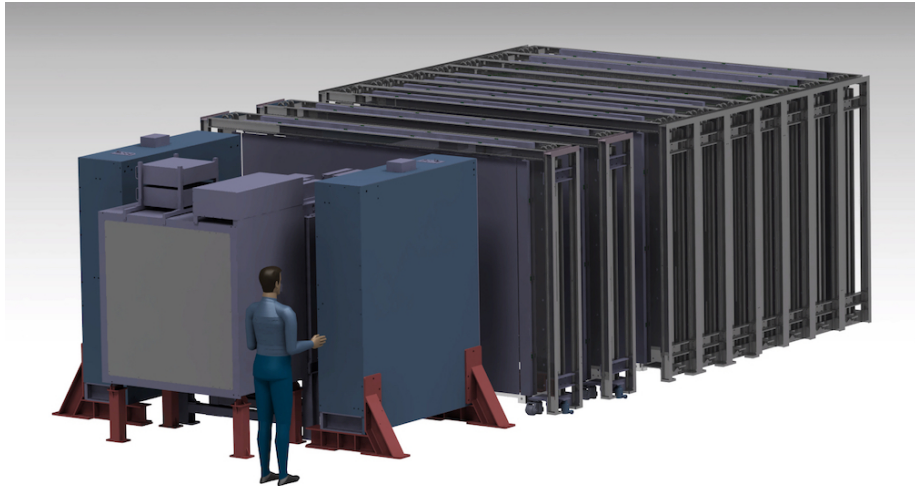


Figure 1: Schematic view of entire sets of detectors.

125 T2K adopted the off-axis beam method, in which the neutrino beam is intentionally
126 directed 2.5 degrees away from SK producing a narrow band ν_μ beam. The off-axis near
127 detector, ND280, is installed towards the SK direction in the B1 floor of the near detector
128 hall of the J-PARC neutrino beam-line. We propose to install our detector in the B2 floor
129 of the near detector hall, where the off-axis angle is similar but slightly different: 1.5 degree.
130 The candidate detector position in the B2 floor is shown in Fig. 3. The expected neutrino
131 energy spectrum at the candidate position is shown in Fig. 4.

132 **2.1 Wagasci modules**

133 **2.1.1 Detector**

134 The WAGASCI modules are mainly composed of 1280 plastic scintillator bars and a sur-
135 rounding stainless steel tank as shown in Fig. 5. The total number of channels in one
136 Wagasci module is 1280. The stainless steel tank is constructed by welding stainless steel
137 plates, is sized as $46 \times 125 \times 125$ cm³, and weighs 0.5 ton.

138 One Wagasci module consists of 16 scintillator tracking planes, where each plane is an

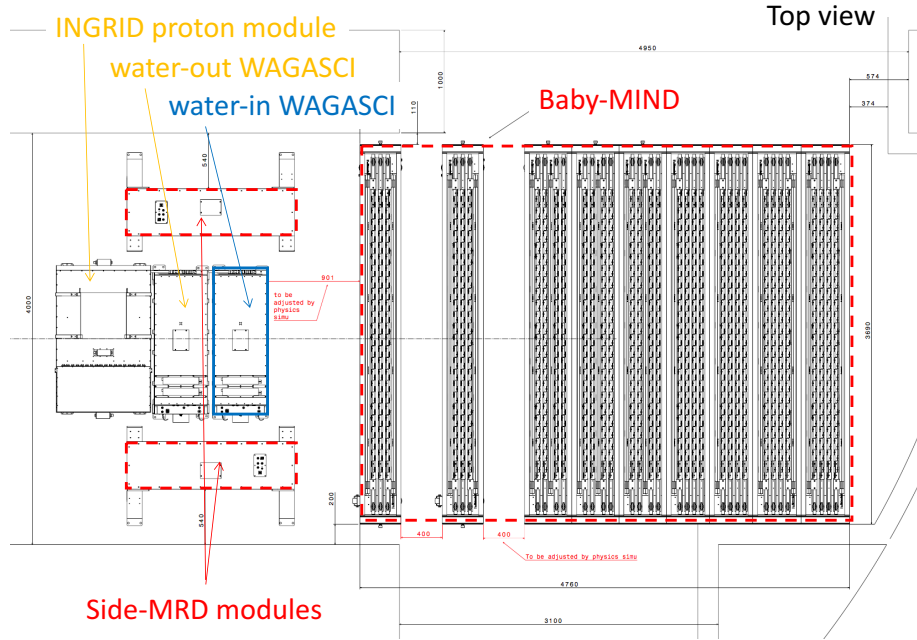


Figure 2: Top view of entire sets of detectors.

array of 80 scintillator bars fixed with ABS frames. The 40 bars, called parallel scintillators, are placed perpendicularly to the beam, and the other 40 bars, called grid scintillators, are placed in parallel to the beam with grid structure in the tracking plane as shown in Fig. 5. Thanks to the 3 D grid-like structure of the scintillator bars, the Wagasci module has 4π angular acceptance for charged particles.

Thin plastic scintillator bars produced at Fermilab by extrusion method, mainly consists of polystyrene and are surrounded by thin reflector including TiO^2 (3 mm in thickness) are used for the Wagasci modules to reduce the mass ratio of scintillator bars to water, because neutrino interactions in the scintillator bars are a background for the cross section measurements on H_2O . Each scintillator bar is sized as $1020 \times 25 \times 3 \text{ mm}^3$ including the reflector part, and half of all the scintillator bars have 5-cm-interval slits to form the grid structure (Figure 6).

We will have two types of the Wagasci modules, a water-in module and a water-out module. The water-in Wagasci module has water in spaces of the grid structure. The total water mass serving as neutrino targets in the fiducial volume of the module is 188 kg, and the mass ratio of scintillator bars to water is 80 %. The water-out Wagasci module doesn't have water inside the detector. The total CH mass serving as neutrino target in the fiducial volume of the module is 47 kg, and the mass fraction of scintillator bars is 100 %.

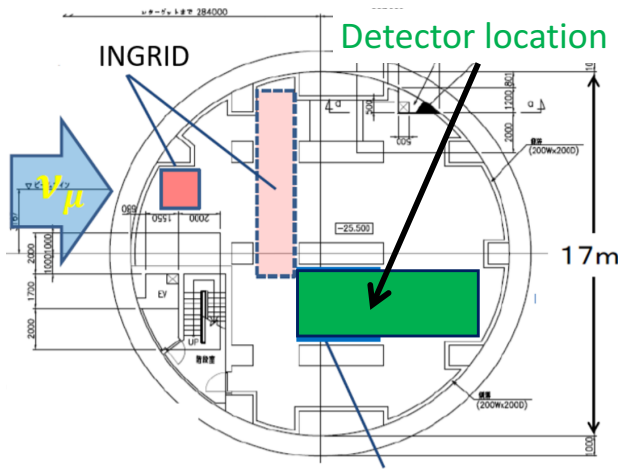


Figure 3: Candidate detector position in the B2 floor of the near detector hall.

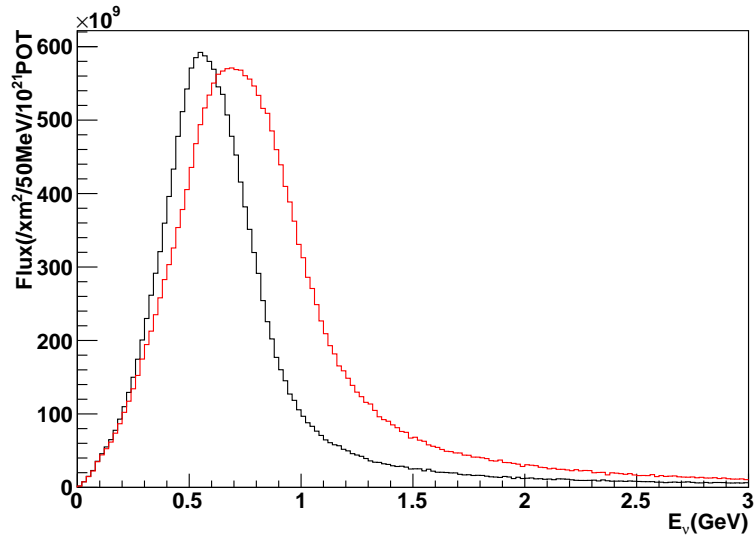


Figure 4: Neutrino energy spectrum at the candidate detector position (red, off-axis 1.5 degree). The spectrum at the ND280 site (black, off-axis 2.5 degree) is also shown.

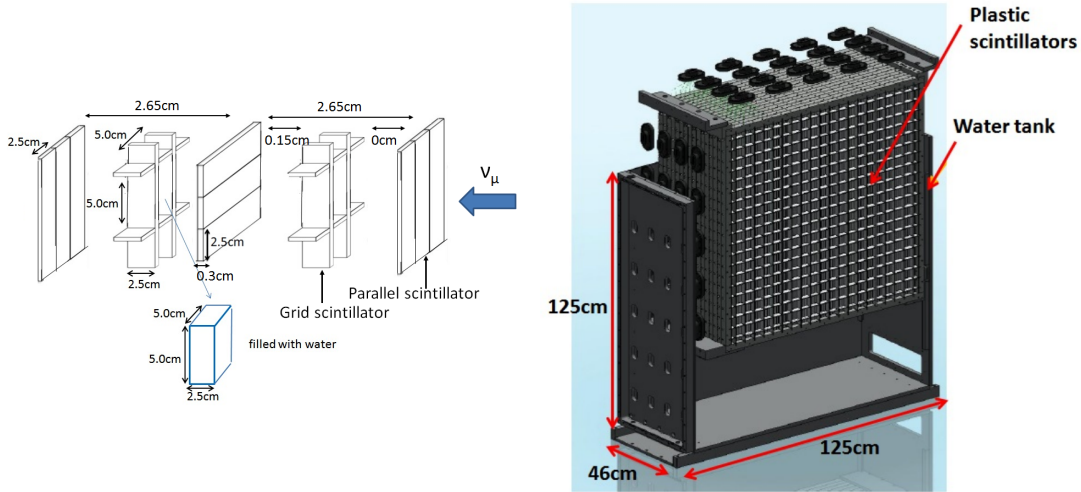


Figure 5: Schematic views of 3D grid-like structure of plastic scintillator bars (left) and Wagasci module (right).

157 Scintillation light is collected by wave length shifting fibers, Y-11 (non-S type with a
 158 diameter of 1.0 mm produced by Kuraray. A fiber is glued by optical cement in a groove
 159 on surface of a scintillator bar. 32 fibers are gathered together by a fiber bundle at edge
 160 of the module, and lead scintillation light to a 32-channel arrayed MPPC. Since crosstalk
 161 of light yield due to reflection on the inner surface of each cell has been observed, all the
 162 scintillator bars are painted black by aqueous color spray. It is confirmed by measurements
 163 with cosmic rays that black painting on the surface of the scintillator bars suppresses this
 164 crosstalk so that no significant crosstalk effect is observed within uncertainty.

165 32-channel arrayed MPPCs, as shown in the Fig. 7, are used for the modules. The
 166 surface of the fiber bundle is polished and directly attached onto the 32-channel arrayed
 167 MPPCs. The positions of 32 fibers on the bundle are aligned to fit the channels of MPPCs.
 168 The MPPC is a product of Hamamatsu Photonics, S13660(ES1), with suppressed noise
 169 rate of ~ 6 kHz per channel at 0.5 p.e. threshold. For each MPPC channel, 716 pixels of
 170 APD are aligned in a shape of circle.

171 2.1.2 Electronics

172 As front-end electronics of this detector, a Silicon PM Integrated Read-Out Chip (SPIROC)
 173 [12] is adopted. SPIROC is a 36-channel auto-triggered front-end ASIC, and is produced
 174 by OMEGA/ IN2P3. It not only contains an analog signal processing part such as amplifi-
 175 cation and shaping of the waveform, but contains a digital signal processing parts such as
 176 auto-trigger and timing measurement. Charge of MPPC signal is sampled by track-and-

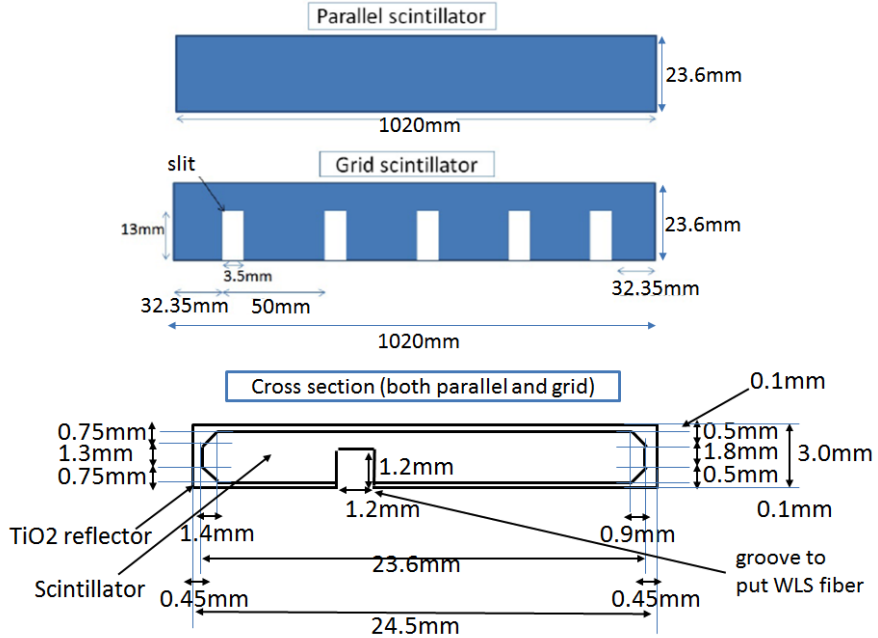


Figure 6: Geometry of scintillators used for Wagasci modules.

hold circuit. A Front-end electronics board, Active Sensor Unit (ASU), has been developed with the SPIROC2D chip, which is the latest version of SPIROC. Each readout board is designed to control a 32-channel arrayed MPPC, and 40 of the ASU boards are aligned on the module surface. The data acquisition system used for this detector, including back-end boards, has been developed for prototypes of ultra-granular calorimeters for the International Linear Collider (ILC) [5], and independent of the T2K DAQ system. To synchronize the DAQ system to J- PARC neutrino beam, pre-beam trigger and beam trigger are sent to the clock control card. The beam trigger signals are converted from optical signals to NIM signals at NIM module on the B2 floor. In addition, the information of spill number are delivered with 16-bit ECL level signals, and converted to an Ethernet frame by an FPGA evaluation board to be directly sent to the DAQ PC. The electronics readout scheme is shown in Fig. 8.

2.1.3 Water system

Pure water is filled to the water tank of the water-in Wagasci module as follows. First, the water storage tank located at the B2 floor of the NM pit is filled with water delivered from a water tap on the ground level through a long hose. Second, the water is pumped to the other water storage tank though a water filler to produce pure water. Third, a

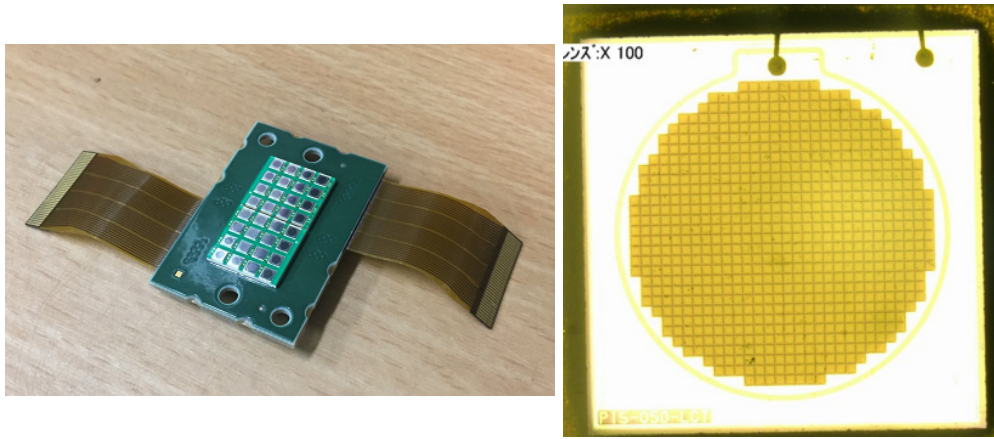


Figure 7: 32-channel arrayed MPPC (left) and an enlarged view of one MPPC channel (right).

194 compound preservative called Germall plus, which is the same preservative used in one of
 195 the sub-detectors of T2K ND280, FGD2, is put into the water to keep water from being
 196 bad. Then, the water is poured to the water-in Wagasci module, and it is kept in the
 197 module during the neutrino beam operation and not to be circulated.

198 **2.2 INGRID Proton module**

199 INGRID Proton module is a neutrino detectors of the T2K experiment. It is a fully-active
 200 tracking detector which consists of only scintillator strips. The purpose of this Proton
 201 Module is to separate the neutrino interaction types by detecting the protons and pions
 202 together with the muons from the neutrino interactions, and to measure the neutrino cross
 203 section for each interaction type. It consists of 36 tracking planes surrounded by veto planes
 204 (Figure 9), where each tracking plane is an array of two types of scintillator strips. The
 205 16 strips in the inner region have dimensions of $2.5\text{cm} \times 1.3\text{cm} \times 120\text{cm}$, while the 16 strips
 206 in the outer region have dimensions of $5\text{cm} \times 1\text{cm} \times 120\text{cm}$, making a plane of $120 \times 120\text{cm}^2$
 207 in the horizontal and vertical directions. The former is the scintillator produced for the
 208 K2K SciBar detector [3] and the latter was produced for INGRID. The tracking planes are
 209 placed perpendicular to the beam axis at 23mm intervals. Since the strips are aligned in one
 210 direction, each tracking plane is sensitive to either the horizontal or vertical position of the
 211 tracks. The tracking planes are therefore placed alternating in the horizontal and vertical
 212 directions so that three-dimensional tracks can be reconstructed. The tracking planes also
 213 serve as the neutrino interaction target. As with the Wagasci modules, scintillation light
 214 is read out by a WLS fiber and MPPC.

215 It was installed at the neutrino beam axis on the SS floor of the T2K near detector hall

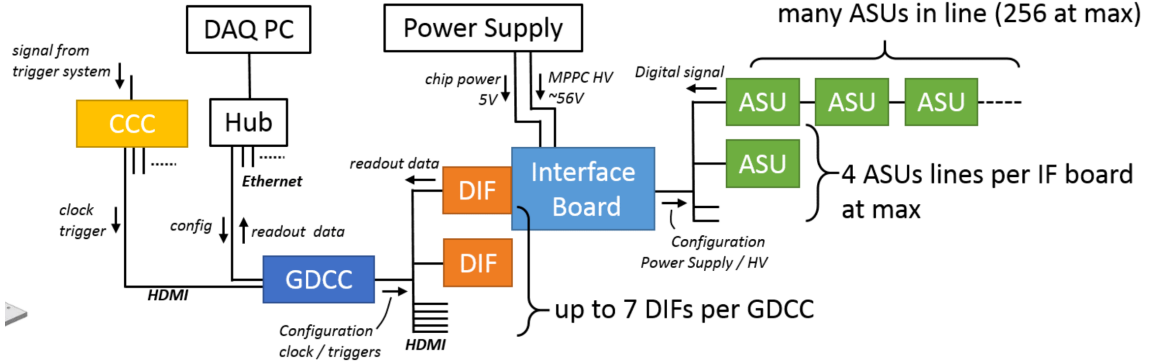


Figure 8: Wagasci electronics readout scheme.

in 2010, and had been used for neutrino cross section measurements. In August 2017, it was moved to the B2 floor of the T2K near detector hall by J-PARC T59 after getting the approval from T2K to use them. J-PARC T59 is performing a neutrino beam measurement using the detector from October 2017, and the measurement will continue until May 2018 as we will discuss in Sec. 4.

We will operate the INGRID Proton module using the T2K near detector electronics/DAQ system in the same way as J-PARC T59. A proposal to use the module and its electronics for our project will be submitted to the T2K collaboration.

2.3 Baby MIND

The Baby MIND is the downstream Muon Range Detector. It also works as a magnet and provides the charge identification capability as well as magnetic momentum measurement for high energy muons.

The Baby MIND collaboration ¹ submitted a proposal to the SPSC at CERN, SPSC-P-353. The project was approved by the CERN research board as Neutrino Platform project NP05 and constructed. The detector consists of 33 magnet modules, each 3500 mm × 2000 mm × 50 mm (30 mm steel) with a mass of approximately 2 tonnes. Of these magnet modules, 18 are instrumented with plastic scintillator modules.

2.3.1 Magnet modules

The Baby MIND is built from sheets of iron interleaved with scintillator detector modules but unlike traditional layouts for magnetized iron neutrino detectors (e.g. MINOS) which tend to be monolithic blocks with a unique pitch between consecutive steel segments and large conductor coils threaded around the whole magnet volume, the Baby MIND iron

¹Contact person: E. Noah, Spokesperson: A. Blondel, Deputy spokesperson: Y. Kudenko



Figure 9: Schematic view of INGRID Proton module.

238 segments are all individually magnetized as shown in Fig. 10, allowing for far greater
 239 flexibility in the setting of the pitch between segments, and in the allowable geometries
 240 that these detectors can take.

241 The key design outcome is a highly optimized magnetic field map. A double-slit con-
 242 figuration for coil winding was adopted to increase the area over which the magnetic flux
 243 lines are homogeneous in B_x across the central tracking region. Simulations show the
 244 magnet field map to be very uniform over this central tracking region covering an area of
 245 $2800 \times 2000 \text{ mm}^2$, Fig. 11. The B_x component dominates in this region, with negligible
 246 B_y and B_z . This was confirmed by measuring the field with 9 pick-up coils wound around
 247 the first module. Subsequent modules were equipped with one pick-up coil. Test results
 248 on the 33 modules show all to achieve the required field of 1.5 T for a current of 140 A,
 249 with a total power consumption of 11.5 kW. The polarity of the field map shown in Fig. 11
 250 (middle) can be reversed by changing the power supply configuration.

251 **2.3.2 Scintillator modules**

252 Each of the 18 scintillator modules is constructed from 2 planes of horizontal counters (95
 253 counters in total) and 2 planes of vertical counters (16 counters in total) [2], arranged
 254 with an overlap between planes to achieve close to 100% hit efficiency for minimum ioniz-

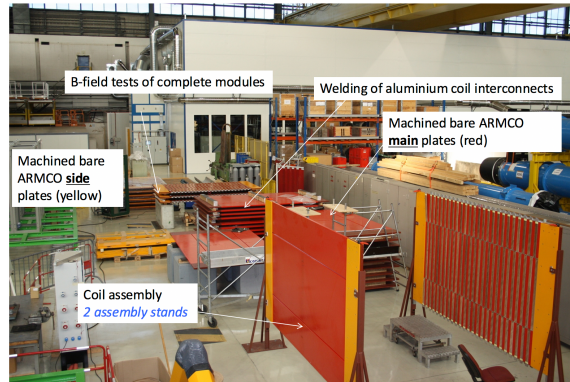


Figure 10: Magnet assembly zone at CERN.

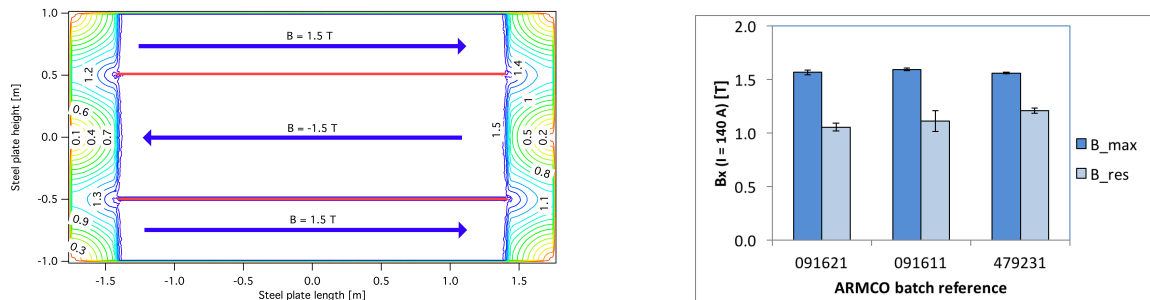


Figure 11: Left) Magnetic field map with a coil along 280 cm of the length of the plate. Right) Measured B field for 33 modules.

255 ing muons. The arrangement of planes within a module is vertical-horizontal-horizontal-
 256 vertical. This arrangement was the result of an assembly approach whereby each plane
 257 was built from 2 half-planes, with each half plane consisting of a horizontal plane and a
 258 vertical plane. The scintillator bars are held in place using structural ladders that align
 259 and maintain the counters, Fig. 12. No glue is used in the process, so counters can be
 260 replaced. Aluminum sheets front and back provide light tightness.



Figure 12: Scintillator modules assembly. Left) top of front half-module showing vertical counters, and the spacers-ladders that set the pitch between horizontal counters and hold them in place. Middle) rear half-module showing horizontal counters on their ladders. Right) Assembled rear half-module, the front half-module can be seen in the background.

261 The plastic scintillator counters were made from 220 mm-wide slabs, consisting of
 262 extruded polystyrene doped with 1.5% paraterphenyl (PTP) and 0.01% POPOP. They were
 263 cut to size then covered with a 30-100 μm thick diffuse reflector resulting from etching of
 264 the surface with a chemical agent [9, 10]. The horizontal counter size is $2880 \times 31 \times 7.5 \text{ mm}^3$,
 265 with one groove along the length of the bar in which sits a wavelength shifting fiber from
 266 Kuraray. The vertical counter size is $1950 \times 210 \times 7.5 \text{ mm}^3$, with one U-shaped groove
 267 along the bar. On each counter, two custom connectors house silicon photomultipliers,
 268 MPPC type S12571-025C from Hamamatsu, either side of the horizontal counter, and
 269 both connectors at the top for the vertical counter. This geometrical configuration for
 270 vertical counters was chosen for ease of connectivity to the electronics, and maintenance
 271 operations.

272 A total of 1744 horizontal counters and 315 vertical counters (including spares) were
 273 produced at the Uniplast company (Vladimir, Russia).

274 2.3.3 Electronics

275 The Baby MIND electronic readout scheme includes several custom-designed boards [11].
 276 The revised version is shown in Fig. 13. At the heart of the system is the electronics
 277 Front End Board (FEB), developed by the University of Geneva. The readout system
 278 includes two ancillary boards, the Backplane, and the Master Clock Board (MCB) whose
 279 development has been managed by INRNE (Bulgarian Academy of Sciences) collaborators.

280 The FEBv2 hosts 3 CITIROC chips that can each read in signals from 32 SiPMs [6].

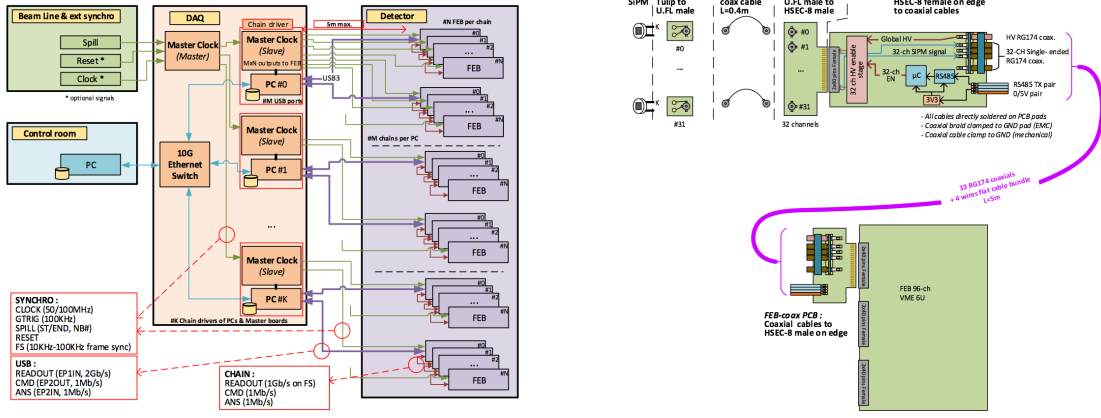


Figure 13: Left) Baby MIND electronics readout scheme. Right) SiPM-to-FEB connectivity.

281 Each signal input is processed by a high gain, and a separate low gain, signal path. The
 282 outputs from the slow shapers can be sampled using one of two modes: a mode with an
 283 externally applied delay, and a peak detector mode. A faster shaper can be switched to
 284 either HG or LG paths, followed by discriminators with adjustable thresholds providing 32
 285 individual trigger outputs and one OR32 trigger output. An Altera ARIA5 FPGA on the
 286 FEBv2 samples these trigger outputs at 400 MHz, recording rising and falling times for
 287 the individual triggers and assigning time stamps to these. Time-over-threshold from the
 288 difference between falling and rising times gives some measure of signal amplitude, used in
 289 addition to charge information and useful if there is more than one hit per bar within the
 290 deadtime due to the readout of the multiplexed charge output of $\sim 9 \mu\text{s}$. The ARIA5 also
 291 manages the digitization of the sampled CITIROC multiplexed HG and LG outputs via a
 292 12-bit 8-ch ADC.

293 The internal 400 MHz clock on the FEBv2 can be synchronized to a common 100 MHz
 294 clock. The synchronization subsystem combines input signals from the beam line into
 295 a digital synchronization signal (SYNC) and produces a common detector clock (CLK)
 296 which can eventually be synchronised to an external experiment clock. Both SYNC and
 297 CLK signals are distributed to the FEBs. Tests show the FEB-to-FEB CLK(SYNC) delay
 298 difference to be 50 ps (70 ps). Signals from the beam line at WAGASCI include two
 299 separate timing signals, arriving 100 ms and 30 μs before the neutrino beam at the near
 300 detectors. The spill number is available as a 16-bit signal.

301 2.3.4 Pefromance check

302 All counters were measured at INR Moscow with a cosmic ray setup using the same type
 303 S12571-025C MPPCs and CAEN DT5742 digitizer. The average light yield (sum from both

304 ends) was measured to be 37.5 photo-electrons (p.e.) per minimum ionizing particle (MIP)
 305 and 65 p.e./MIP for vertical and horizontal counters, respectively. After shipment to
 306 CERN, all counters were tested once more individually with an LED test setup [?]. 0.1% of
 307 counters failed the LED tests and were therefore not used during the assembly of modules.
 308 The assembly of modules was completed in June 2017, and it was then tested in June and
 309 July 2017 at the Proton Synchrotron experimental hall at CERN with a mixed particle
 310 beam comprising mostly muons whose momenta could be selected between 0.5 and 5 GeV/c.
 An event display from the summer 2017 tests is shown in Fig. 14.

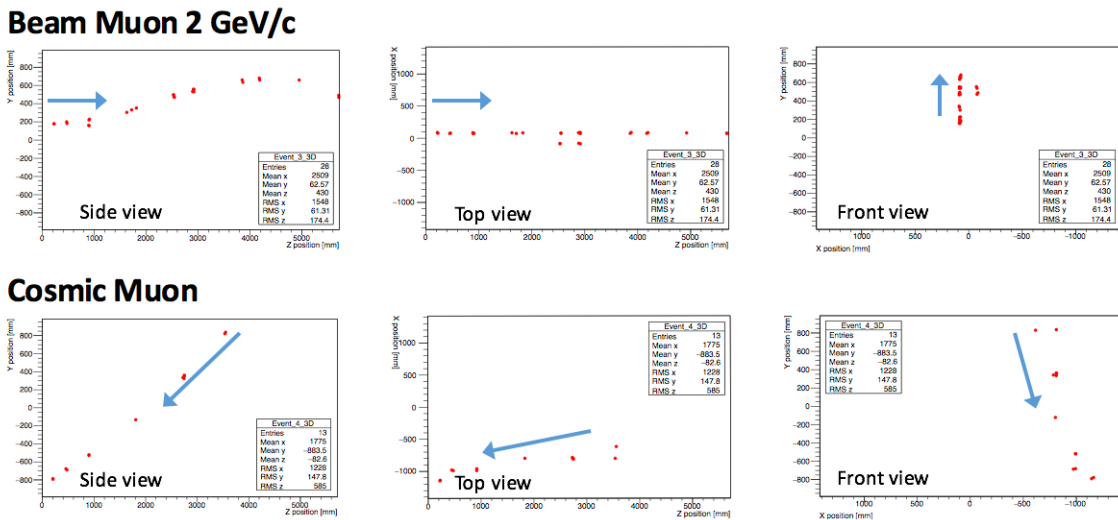


Figure 14: Comparison of a beam muon and cosmic muon in the three different geometrical projections of the detector. The beam impinges on the detector from the left. The arrows indicate the direction of travel of these muons. The direction of the cosmic muon is inferred from timing information.

311

312 2.4 Side muon range detector

313 Two Side-MRD modules for tracking secondary particles from neutrino interactions will be
 314 installed in 2018. Each Side-MRD module is composed of 11 steel plates and 10 layers of
 315 total 80 scintillator slabs installed in 13 mm gaps between the 30 mm thick plates. Each
 316 steel plate size is $30 \times 1610 \times 1800 \text{ mm}^3$. Total module size is $2236 \times 1630 \times 975 \text{ mm}^3$ as
 317 shown in Fig. 15 (left), weight is ~ 8.5 ton.

318 Scintillator bars were manufactured by Uniplast company in Vladimir, Russia. Polystyrene
 319 based scintillators were extruded with thickness of 7 mm, then cut to the size of $7 \times 200 \times$
 320 1800 mm^3 . Dopant composition is 1.5% PTP and 0.01% POPOP. Scintillator surface was
 321 etched by a chemical agent to form a white diffuse layer with excellent reflective perfor-

322 mance. Ideal contact between the scintillator and the reflector raises the light yield up to
 323 50% comparing to an uncovered scintillator. Sine like groove was milled along the scin-
 324 tillator to provide uniform light collection over the whole scintillator surface. WLS Y11
 325 Kuraray fiber of 1 mm diameter is glued with an optical cement EJ-500 in the S-shape
 326 groove as shown in Fig. 15(right). Bending radius is fixed to 30 mm that was specified to
 327 be safe for Kuraray S-type fibers. Both ends of the fiber are glued into optical connectors
 328 which mounted within a scintillator body and provide an interface to SiPMs, Hamamatsu
 329 MPPC S13081-050CS(X1).

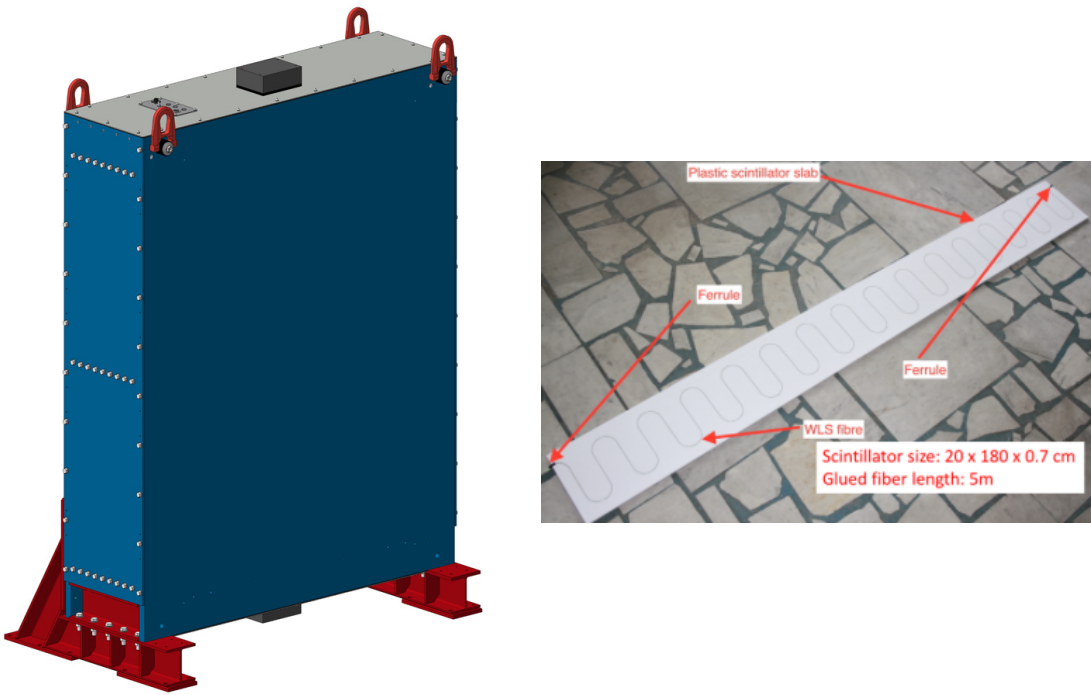


Figure 15: Left :Side-MRD module. Right: Scintillator bar of the Side-MRD modules.

330 Scintillators for the Side-MRD modules had been assembled at INR in Russia, and
 331 shipped to Japan in July 2017. The light yield for each scintillator was measured with
 332 cosmic rays at INR and at YNU in Japan after delivery. Parameters measured at the
 333 center of the counter were : the light yields LY_1 and LY_2 at both ends, the light yield
 334 asymmetry between the ends calculated as $100\% \times \frac{LY_1 - LY_2}{LY_1 + LY_2}$. After tests at INR we selected
 335 324 counters from measured 332 ones with the mean light yield of 45 p.e./MIP ($LY_1 + LY_2$
 336) and the asymmetry value less than 10 %. The measuremens at YNU yielded the average
 337 total light yield of about 40 p.e./MIP which varies in range from 32 to 50 p.e./MIP (Fig.

338 16 (left)). Only two counters showed relatively high asymmetry close to 25 % as shown in
 339 Fig. 16 (right). Using the results of the quality assurance test we selected 320 scintillator
 340 counters for the Side-MRD modules.

341 We also measured the time resolution for a combination of four counters piled each on
 342 another one. The average result for four counters is $\sigma_T = 1.04$ ns. The resolution of com-
 343 bination of 2, 3, 4 counters is measured to be 0.79 ns, 0.66 ns and 0.58 ns, correspondently.

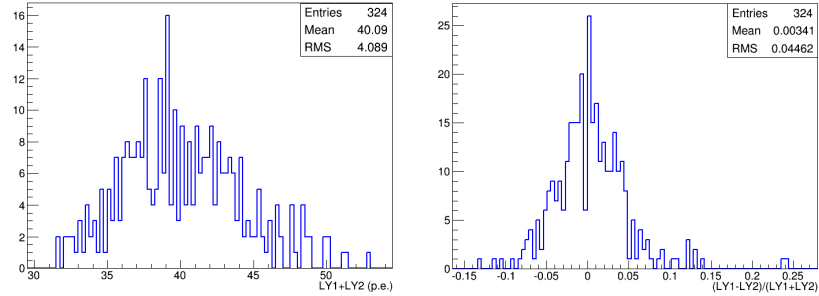


Figure 16: Total light yield distribution (left) and light yield assymetry (right) measured at YNU.

344
 345 Construction of Side-MRD modules will be done from November 2017 at Yokohama
 346 National University, then they will be transported to J-PARC and will be installed at B2
 347 floor of the T2K near detector hall.

348 Same electronics as the WAGASCI modules (see Sec. 2.1.2) are used for the Side-MRD
 349 modules.

350 3 Physics goals

351 We will measure the differential cross section for the charged current interaction on H_2O
 352 and Hydrocarbon(CH)). The water-scintillator mass ratio of the Wagasci module is as
 353 high as 5:1 and the high purity measurement of the cross section on H_2O is possible. One
 354 experimental option is to remove water from one of the two Wagasci modules. The water-
 355 out WAGASCI module will allow to measure pure-CH target interactions with very low
 356 momentum-threshold for protons. It will also benefit to subtract the background from
 357 interaction with scintillator in the water target measurement. Another option is to add
 358 the T2K proton module which is fully made of plastic scintillators. It will allow the high
 359 statistics comparison of cross section between H_2O and CH and also comparison with
 360 the ND280 measurement. The actual configuration will be optimized with detailed MC
 361 simulation by 2018 Summer.

Our setup allows the measurements of inclusive and also exclusive channels such as $1-\mu$, $1-\mu 1p$, $1-\mu 1\pi \pm np$ samples, former two of which are mainly caused by the quasi-elastic and 2p2h interaction and the latter is mainly caused by resonant or coherent pion production and deep elastic scattering. In general, an accelerator produced neutrino beam spectrum is wide and the energy reconstruction somehow rely on the neutrino interaction model. Therefore, recent neutrino cross section measurement results including those from T2K are given as a flux-integrated cross section rather than cross sections as a function of the neutrino energy to avoid the model dependency. We can provide the flux-averaged cross section. In addition, by combining our measurements with those at ND280, model-independent extraction of the cross section for narrow energy region becomes possible. This method was demonstrated in [1] and also proposed by P** (NUPRISM).

3.1 Expected number of events

Expected number of neutrino events after the event selections is evaluated with Monte Carlo simulations as we will discuss in Section 5. In the neutrino-mode, 4.2×10^3 , 1.1×10^3 and 3.8×10^3 CC neutrino events are expected in the water-in WAGASCI module, the water-out WAGASCI module and the INGRID proton module after the selections with 0.5×10^{21} POT, and its purities are 78.0 %, 97.5 % and $\sim 98\%$. In the antineutrino-mode, 1.7×10^3 , 0.4×10^3 and 1.5×10^3 CC antineutrino events are expected in the water-in WAGASCI module, the water-out WAGASCI module and the INGRID proton module after the selections with 0.5×10^{21} POT, and its purities are 59.5 %, 74.4 % and $\sim 74\%$.

Statistical errors of flux integrated CC-inclusive neutrino cross section measurements on H_2O (full acceptance) and CH targets (forward acceptance) will be 1.5 % and 1.6 % with 0.5×10^{21} POT in the neutrino-mode. Statistical errors of flux integrated CC-inclusive antineutrino cross section measurements on H_2O (full acceptance) and CH targets (forward acceptance) will be 2.4 % and 2.5 % with 0.5×10^{21} POT in the antineutrino-mode.

Statistical errors of flux integrated H_2O to CH CC-inclusive neutrino cross section ratio measurement will be 3.1 % (full acceptance) and 2.3 % (forward acceptance) with 0.5×10^{21} POT in the neutrino-mode. Statistical errors of flux integrated H_2O to CH CC-inclusive antineutrino cross section ratio measurement will be 5 % (full acceptance) and 3.7 % (forward acceptance) with 0.5×10^{21} POT in the antineutrino-mode.

3.2 Pseudo-monochromatic beam by using different off-axis fluxes

The off-axis method gives narrower neutrino spectrum, and the peak energy is lower for larger off-axis angle. There still remains high energy tail mainly due to neutrinos from Kaon decay. The off-axis angle of the Wagasci location is 1.5 degree and different from the ND280 2.5 degree. Top two plots of Fig. 17 show the energy spectra of fluxes and neutrino interaction events at these two different location. The high energy tail of ND280 flux can be somehow subtraction by using the Wagasci measurement. The low energy part of the

399 Wagasci flux can be also subtracted by using the ND280 measurement. Bottom two plots
400 of Fig. 17 demonstrate this method. We can effectively get two fluxes, from 0.2 GeV to
401 0.9 GeV and 0.6 GeV and 2 GeV and measure flux-integrated cross section for these two
402 fluxes.

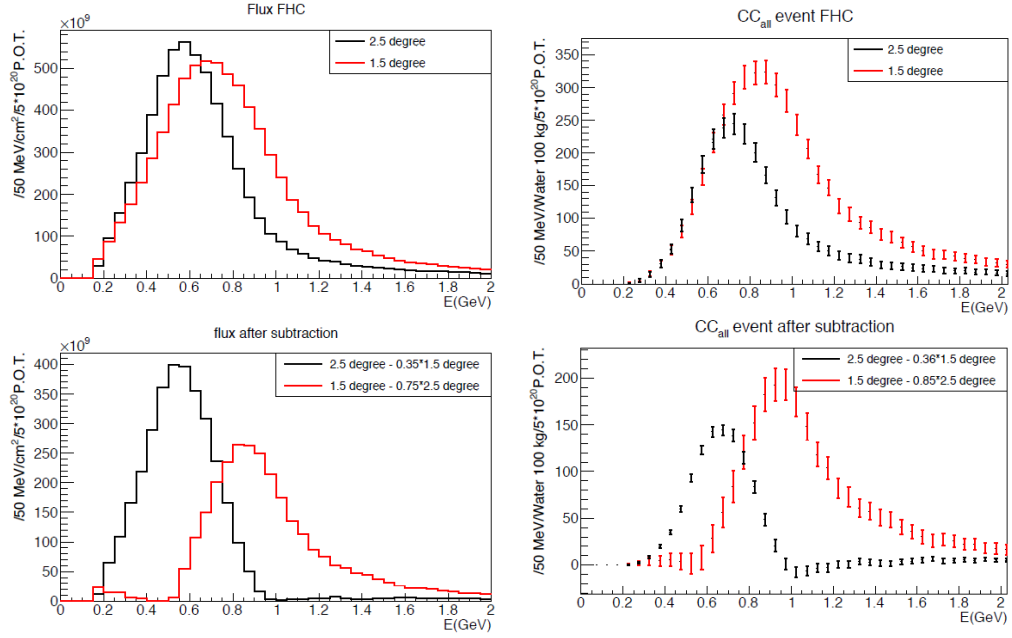


Figure 17: Energy spectra obtained by using different off-axis angle fluxes. Top two plots show the fluxes(left) and spectra of interaction events (right) for ND280 (off-axis 2.5 degree) and Wagasci (off-axis 1.5 degree). Bottom two plots show the fluxes (left) and spectra of interaction events (right) obtained by subtraction of fluxes at ND280 and Wagasci. The error bar is for the statistical error and those in the bottom right plot is obtained assuming the statistical error for ND280 measurement is much smaller than that of Wagasci experiment.

403 Statical errors of flux integrated CC-inclusive neutrino cross section measurements
404 on H₂O (forward acceptance) and CH targets (forward acceptance) with the pseudo-
405 monochromatic beam will be 2 % and 1.9 % with 0.5×10^{21} POT in the neutrino-mode.
406 Statical errors of flux integrated CC-inclusive antineutrino cross section measurements
407 on H₂O (forward acceptance) and CH targets (forward acceptance) with the pseudo-
408 monochromatic beam will be 3 % and 2.8 % with 0.5×10^{21} POT in the neutrino-mode.

409 **3.3 Subjects Wagasci can contribute**

410 In T2K experiment, neutrinos interact with bound nucleons in relatively heavy nuclei
411 (Carbon and Oxygen), so the cross-section is largely affected by nuclear effects. The nuclear
412 effects are categorized as nucleons' momentum distribution in nucleus, interactions with
413 correlated pairs of nucleons in nucleus (two particles-two holes, 2p2h), collective nuclear
414 effects and final state interactions (FSI) of secondary particles in the nuclei after the initial
415 neutrino interactions.

416 The 2p2h interactions mainly happen through Δ resonance interactions following a
417 pion-less decay and interactions with a correlated nucleon pair. The 2p2h interactions are
418 observed in electron scattering experiments [7] where the 2p2h events observed in the gap
419 between Quasi-Elastic region and Pion-production region as shown in Fig. 18. Neutrino
420 experiments also attempt to measure the 2p2h interactions, but separation of the QE peak
421 and the 2p2h peak is more difficult because transferred momentum (p) and energy (w)
422 are largely affected by neutrino energies which cannot be determined event-by-event in the
423 wide energy spectrum of the accelerator neutrino beam. Our model-independent narrow
424 neutrino spectra extracted from combined analyses of our data and ND280 data are ideal
425 for searching the 2p2h interaction because clearer separation of the QE peak and the 2p2h
426 peak is expected. Another way to observe the 2p2h interaction is direct measurement of
427 proton tracks in CC0 π sample with low detection threshold and full acceptance. Fig. 19
428 shows proton multiplicities after FSI in CCQE events and 2p2h events, and Fig. 20 shows
429 opening angles among two proton tracks in the same samples. The water-out Wagasci
430 can provide good sample for the 2p2h interaction search because its low density medium
431 enables the detection of low momentum protons in addition to the full acceptance.

432 There are various models which describe the collective nuclear effects [8]. The Q^2
433 dependence of the effects can be tested by measuring angular distribution of muons in
434 CC1- μ and CC1- $\mu 1p$ events. The uncertainties of the effects in low (high) Q^2 regions can
435 be constrained by observing the events with a forward-going (high-angle) muon, so it is
436 essential to measure muon tracks with full acceptance.

437 T2K experiment is starting to use ν_e CC1 π events for its CP violation search to increase
438 the statistics. One of the biggest uncertainty of the CC1 π sample comes from the final
439 state interactions of pions in the nuclei after the initial neutrino interactions because they
440 change the multiplicity, charge and kinematics of the pions. The multi-pion production
441 events can be migrated into the CC1 π sample due to the FSIs, and they become important
442 backgrounds. We can constrain the uncertainties from the pion FSIs by measuring pion
443 rescattering in the detector and pion multiplicity in ν_μ CCn π sample with low detection
444 threshold and full acceptance for pion tracks. The water-out WAGASCI can provide good
445 sample for the pion FSI studies because its low density medium enables the detection of
446 low momentum pions in addition to the full acceptance.

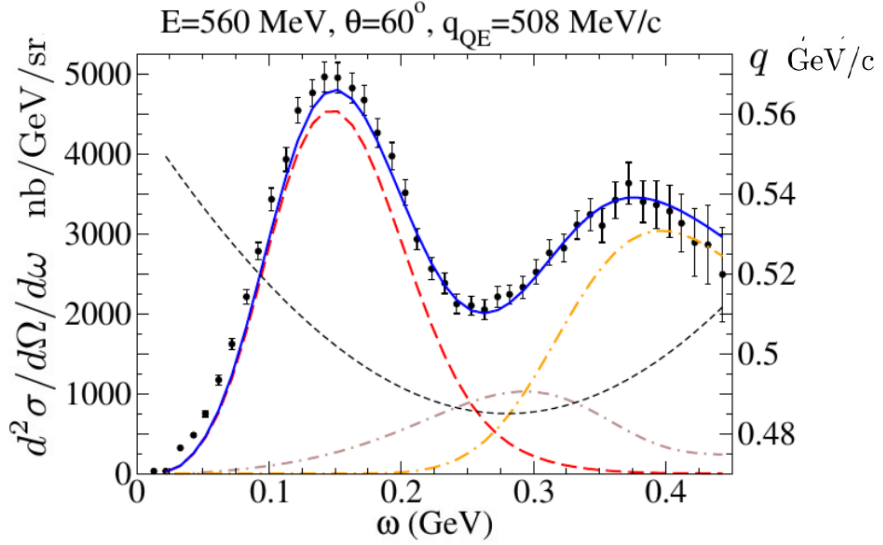


Figure 18: Comparison of inclusive $^{12}\text{C}(e,e')$ cross sections and predictions of the QE-SuSAv2 model (long-dashed red line), 2p-2h MEC model (dot-dashed brown line) and inelastic-SuSAv2 model (long dot-dashed orange line) (from Ref. [7]). The sum of the three contributions is represented with a solid blue line. The q dependence with w is also shown (short-dashed black line.)

4 Status of J-PARC T59 experiment

We had submitted a proposal of a test experiment to J-PARC in April 2014 to test a new detector with a water target, WAGASCI, at the neutrino monitor hall, and the proposal was approved as J-PARC T59. The project contains the side and downstream muon range detectors as well.

The first WAGASCI module has been constructed in 2016 and installed at the on-axis position in front of the T2K INGRID detector for the commissioning and the first cross section measurement as a part of the T2K experiment. The INGRID electronics boards are used to read the signal. The light yield measured with muons produced by the interaction of neutrinos in the hall wall, shown in Fig. 21, is sufficiently high to get good hit efficiency. A track search algorithm based on the cellular automaton has been developed using the software tools by the T2K INGRID. Examples of observed events are shown in Fig. 22. The tracking efficiency in 2-dimensional projected plane was evaluated by comparing the reconstructed track in the WAGASCI module and the INGRID module and shown in Fig. 23. Note that the tracking efficiency for high angle (> 70 deg) is not evaluated because of the acceptance of the INGRID module, not because of the limitation

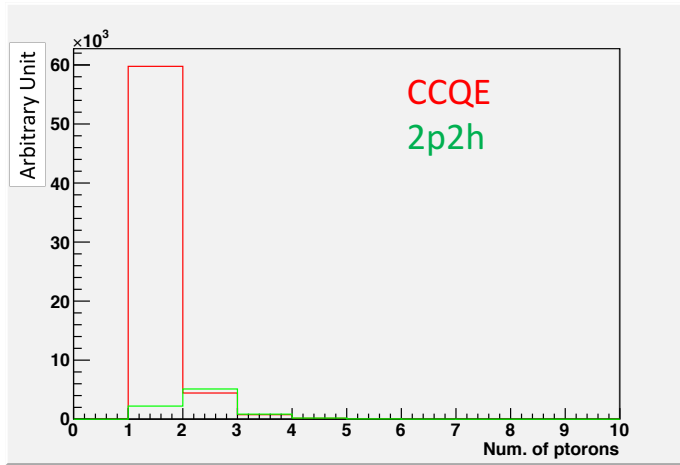


Figure 19: Proton multiplicities after FSI in CCQE events and 2p2h events.

463 of the WAGASCI module.

464 In 2017 Autumn, the construction of the second WAGASCI module and the dedicated
 465 electronics board were completed. The module and the electronics were install to the B2
 466 floor together with the T2K proton module and the INGRID module as shown in Fig. 24.
 467 The proton module is to be used as the entering muon veto and also for the comparison
 468 of interaction between CH and Water. The INGRID module is for the temporary muon
 469 detector with limited acceptance for this period. The detector was commissioned and is
 470 in operation to take data with the antineutrino beam during the T2K beam time from
 471 October.

472 The production of the components of the side muon range detectors has been completed
 473 and now the detectors are being assembled at the Yokohama National University. These
 474 detectors will be installed sometime from January to June, 2018 when T2K is not running.

475 The Baby MIND detector was transported from CERN to Japan in December, 2017.
 476 It will be installed and commissioned in Jan.-Feb. 2018 and T59 will take the neutrino-
 477 induced muon data in April and May.

478 5 MC studies

479 5.1 Detector simulation

480 Expected number of neutrino events in the water-in Wagasci detector is evaluated with
 481 Monte Carlo simulations. Neutrino beam flux at the detector location is simulated by

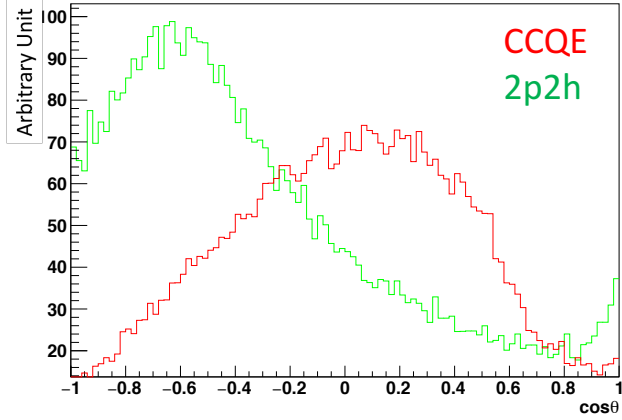


Figure 20: Opening angles among two proton tracks after FSI in CCQE events and 2p2h events.

482 T2K neutrino flux generator, JNUBEAM, neutrino interactions with target materials are
 483 simulated by a neutrino interaction simulator, NEUT, detector responses are simulated
 484 using GEANT4-based simulation. The neutrino flux at the detector location, 1.5 degrees
 485 away from the J-PARC neutrino beam axis, is shown in Figure 4, and its mean neutrino
 486 energy is around 0.68 GeV.

487 **5.1.1 Detector geometry**

488 The detector geometry in the GEANT4-based simulation is slightly different from the actual
 489 detector as shown in Fig. 25. The active neutrino target region consists of four Wagasci
 490 modules, and each Wagasci detector has the dimension with 100 cm \times 100 cm in the x and
 491 y directions and 50 cm along the beam direction. Two Side-MRD modules are installed at
 492 both sides of the Wagasci modules, and each Side-MRD module consists of ten iron plates
 493 whose dimension is 3 cm (thickness) \times 200 cm (height) \times 320 cm (width). The distance
 494 between the Side-MRD modules and Wagasci modules is 80 cm. The downstream-MRD
 495 equivalent to the Baby-MIND is installed at the downstream of the Wagasci modules. The
 496 downstream-MRD consists of thirty iron plates whose dimension is 3 cm (thickness) \times 200
 497 cm (height) \times 400 cm (width). The distance between the downstream-MRD modules and
 498 Wagasci modules is 80 cm.

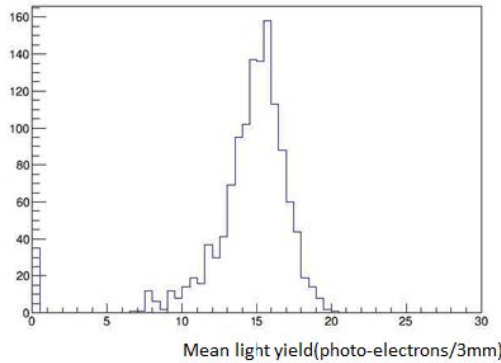


Figure 21: Light yield for muons produced by the interaction of neutrinos in the hall wall. Average light yields for each channel are plotted.

499 **5.1.2 Response of detector components**

500 The energy deposit inside the scintillator is converted into the number of photons. The
 501 effects of collection and attenuation of the light in the scintillator and the WLS fiber are
 502 simulated, and the MPPC response is also taken into account. The light yield is smeared
 503 according to statistical fluctuations and electrical noise.

504 **5.2 Track reconstruction**

505 To select neutrino interaction from the hit patterns, a track reconstruction algorithm is
 506 developed. The flow of the track reconstruction is as follows.

- 507 1. Two-dimensional track reconstruction in each sub-detectors
- 508 2. Track matching among the sub-detectors
- 509 3. Three -dimensional track reconstruction

510 Add explanation about two-dim reco, track matching and three-dim reco here.

511 **5.3 Event selection**

512 First, the events with the track which starts in 5 cm from the wall of the Wagasci module
 513 are rejected to remove the background from the outside.

514 Second, to reject backgrounds from NC and neutral particles, the longest tracks are
 515 required to penetrate more than one (five) iron plates in Side-MRD modules (Baby-MIND).

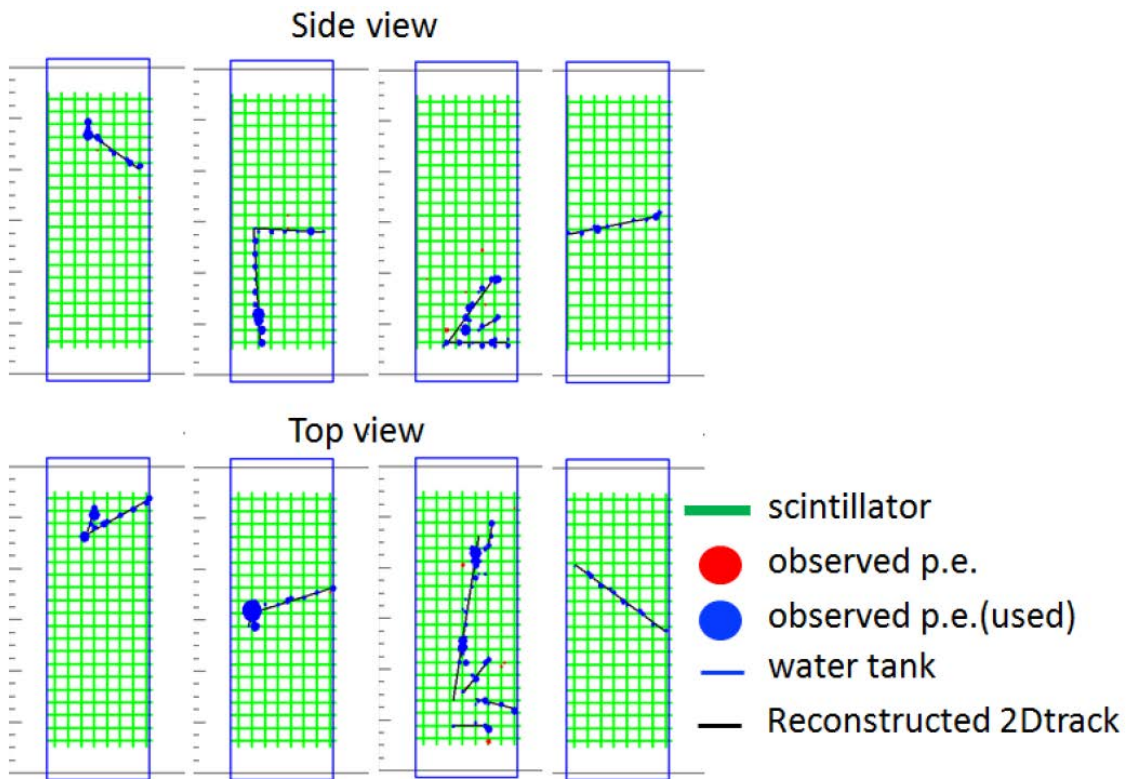


Figure 22: Example event displays of the WAGASCI module at on-axis. The reconstructed tracks are overlaid.

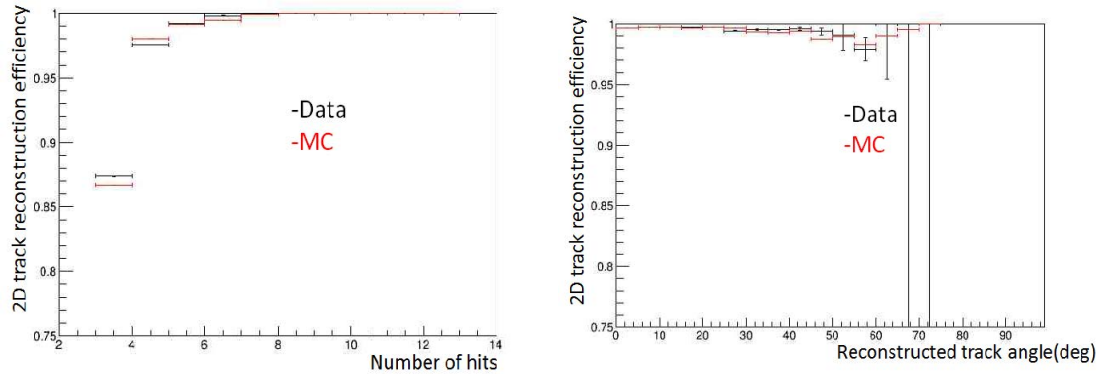


Figure 23: 2D track reconstruction efficiency as a function of number of hits (left) and track angle (right). Here the track angle is the one reconstructed by the INGRID module.

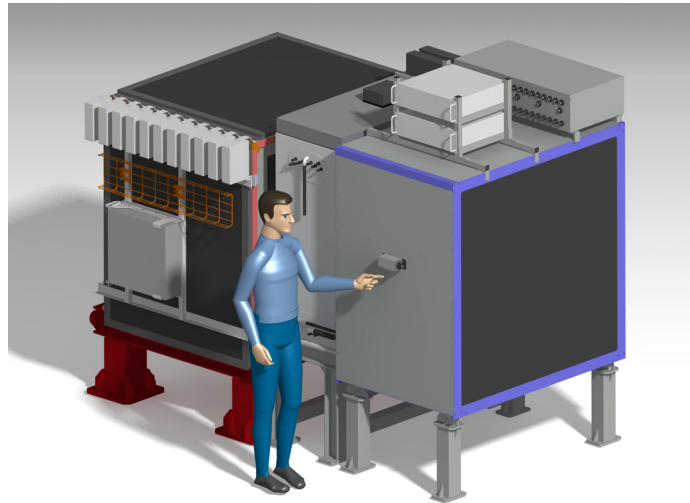


Figure 24: J-PARC T59 detector configuration in October 2017.

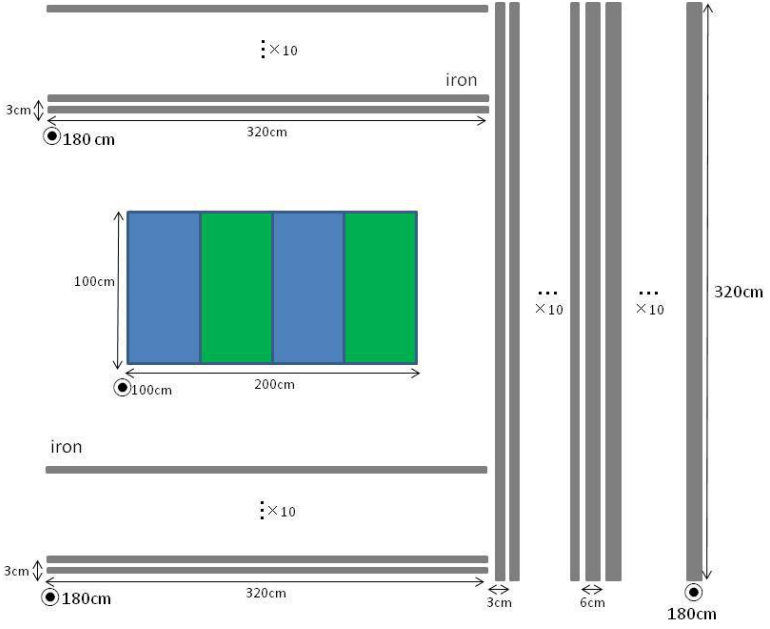


Figure 25: Geometry of the detectors in the Monte Carlo simulation.

516 Then, in order to measure muon momentum, the longest tracks are required to stop in
 517 MRDs (Side-MRD modules and Baby-MIND) or penetrate all iron plates.

518 Table 1 and 2 show numbers of the selected events in one water-in Wagasci module
 519 after each event selection in neutrino-mode and antineutrino-mode respectively. As for
 520 the neutrino-mode, 8478 CC events are expected with 1×10^{21} POT, and the purity is
 521 78.0 %. The main background for the neutrino-mode is the neutrino interactions in the
 522 scintillators inside the Wagasci detector. As for the antineutrino-mode, 3331 CC events
 523 are expected with 1×10^{21} POT, and the purity is 59.5 %. The main background for the
 524 antineutrino-mode is the wrong sign contamination from ν_μ events and the antineutrino
 525 interactions in the scintillators inside the Wagasci detector.

526 Table 3 and 4 show numbers of the charged-current events in the water-in Wagasci
 527 module after all event selection with a classification based on interactions at a vertex with
 528 1×10^{21} POT in neutrino-mode and antineutrino-mode respectively.

529 Table 5 and 6 show numbers of the charged-current events in one water-in Wagasci
 530 module after all event selection with a classification based on particles after final state
 531 interactions with 1×10^{21} POT in neutrino-mode and antineutrino-mode respectively.

532 Figure 26 and 27 show the reconstructed angles of the longest tracks in the selected
 533 events in the neutrino-mode and the anti-neutrino mode respectively. Figure 28, 29 30

Table 1: Expected number of the neutrino-candidate events in one water-in Wagasci module with 1×10^{21} POT in neutrino-mode.

Cut	CC	NC	Scinti Bkg.	Total
Reconstructed	18093.2	699.7	4698.3	23491.2
FV	15150.8	588.4	3934.8	19673.9
Pene. iron	11264.3	237.3	2875.4	14377.0
Stop/Penetrate MRDs	8478.2	214.0	2173.1	10865.2
after all cuts	78.0 %	2.0 %	20.0 %	100 %

Table 2: Expected number of the antineutrino-candidate events in one water-in Wagasci module with 1×10^{21} POT in antineutrino-mode.

Cut	CC	NC	Scinti Bkg.	Wrong sign bkg	Total
Reconstructed	6499.7	107.3	2234.4	2330.8	11172.1
FV	5457.9	89.3	1873.5	1946.6	9367.1
Pene. iron	4172.3	30.8	1440.9	1560.6	7204.6
Stop/Penetrate MRDs	3331.5	28.5	1120.3	1121.2	5601.5
after all cuts	59.5 %	0.5 %	20.0 %	20.0 %	100 %

534 and 31 show the iron plane numbers in Side-MRD and Baby-MIND corresponding to the
 535 end points of the longest tracks in the selected events in the neutrino-mode and the anti-
 536 neutrino mode.

537 5.4 Cross section measurements

538 The flux-averaged ν_μ ($\bar{\nu}_\mu$) CC inclusive cross sections on water and hydrocarbon are calcu-
 539 lated from the number of selected events using the background subtraction and efficiency

Table 3: Expected number of the charged-current events in the water-in Wagasci module after the event selections with 1×10^{21} POT in neutrino-mode with a classification based on interactions at a vertex.

CCQE	MEC	CCRes	CCDIS	Total
3716.3	747.0	2081.3	1132.3	7676.9
48.4 %	9.7 %	27.1 %	14.7 %	100 %

Table 4: Expected number of the charged-current events in the water-in Wagasci module after the event selections with 1×10^{21} POT in antineutrino-mode with a classification based on interactions at a vertex.

CCQE	MEC	CCRes	CCDIS	Total
2522.0	362.8	765.8	765.8	4416.4
hline 57.1 %	8.2 %	17.3 %	17.3 %	100 %

Table 5: Expected number of the charged-current events in one water-in Wagasci module after the event selections with 1×10^{21} POT in neutrino-mode with a classification based on particles after final state interactions.

CC0 π	CC1 π	CC2 π	CCn π	Total
5423.1	1684.3	242.9	701.1	8051.4
67.4 %	20.9 %	3.0 %	8.7 %	100 %

540 correction

$$\sigma_{CC} = \frac{N_{sel} - N_{BG}}{\phi T \epsilon}, \quad (1)$$

541 where N_{sel} is the number of selected events from real data, N_{BG} is the number of selected
542 background events predicted by MC simulation, ϕ is the integrated ν_μ flux, T is the number
543 of target nucleons, and ϵ is the detection efficiency for CC events predicted by MC simula-
544 tion. in the water and hydrocarbon regions in the central detector. Finally, we will cancel
545 the dominant systematic error, the neutrino flux error, by comparing the cross-section re-
546 sults from two neutrino targets, water and hydrocarbon, having almost identical neutrino
547 fluxes, and measure the water to hydrocarbon charged current cross section ratio with 3%
548 precision, which is achieved in the INGRID measurement [4].

549 In the water target events, the background from interaction with scintillators has to be
550 subtracted by using the measurement of the hydrocarbon target.

Table 6: Expected number of the charged-current events in one water-in Wagasci module after the event selections with 1×10^{21} POT in antineutrino-mode with a classification based on particles after final state interactions.

CC0 π	CC1 π	CC2 π	CCn π	Total
2529.3	520.0	37.9	96.0	3183.2
79.5 %	16.3 %	1.2 %	3.0 %	100 %

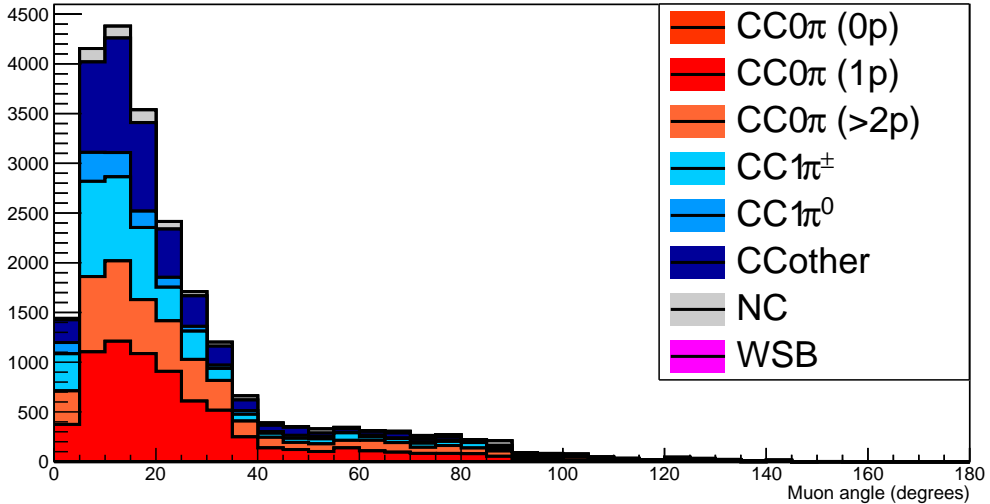


Figure 26: The reconstructed angles of the longest tracks in the selected events in the neutrino-mode.

551 6 Standalone WAGASCI-module performances

552 In the previous sections, the WAGASCI detector was studied using the Muon Range Detectors. In this section, the standalone abilities of WAGASCI module are presented. Using
 553 the WAGASCI configuration presented in Section 5, we have evaluated that only 7% of
 554 the muons will be stopped in one of the WAGASCI modules. THowever, this proportion
 555 increases to 53% for pions and 73% for protons produced by neutrino interactions at 1.5°
 556 off-axis. Figure 32 shows the momentum distribution of these daughter particles as well as
 557 for the sub-sample stopped in one of the WAGASCI modules. Therefore, the study of the
 558 standalone abilities of the WAGASCI module in this section are dominantly motivated by:
 559

- 560 • the accurate measurement of the neutrino interaction final states. Though most of the
 561 muons will be reconstructed and identified in the MRDs, the hadronic particles will
 562 predominantly stops in one WAGASCI module. One has therefore to rely exclusively
 563 on the WAGASCI module information alone to reconstruct, identify and measure the
 564 momentum of pions or protons.
- 565 • the coverage of the MRDs is not 4π . Using the WAGASCI module information can
 566 therefore help to constraint the particles that exits the WAGASCI module but do
 567 not geometrically enters any MRD.

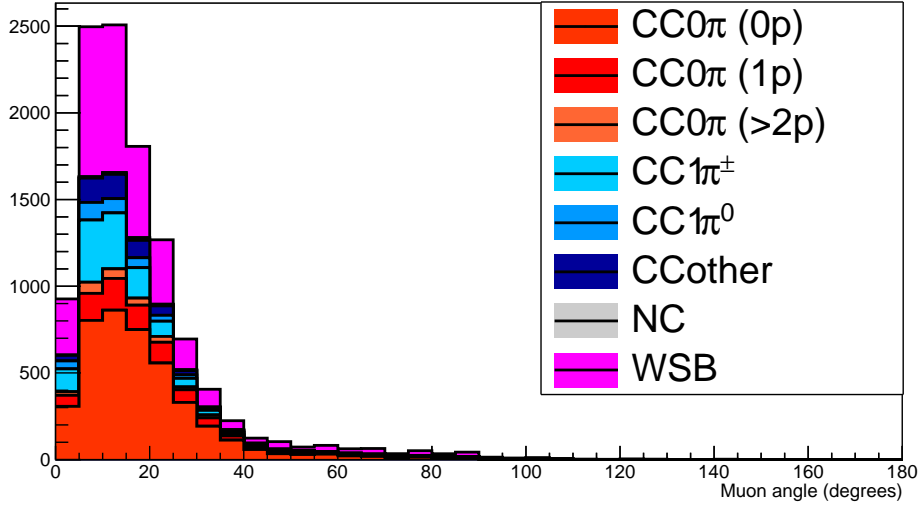


Figure 27: The reconstructed angles of the longest tracks in the selected events in the antineutrino-mode.

- 568 • the particle identification of low momenta $p_\mu < 300$ MeV/c that will leave only
- 569 few hits in the MRD. Using the WAGASCI module information will clearly enhance
- 570 the particle identification.

571 This study is based on an original study done for the ND280 upgrade target, with some
 572 modifications. Though the cell size is similar to the WAGASCI configuration presented
 573 in Section 5, the external dimensions are different ($186.4 \times 60 \times 130$ cm 3). Whenever the
 574 results are presented with this external size and this parameter is likely to impact the
 575 result, it will be mentioned.

576 Note that in this section, a simplified reconstruction algorithm presented in Section 6.1 is
 577 used. The fiducial volume is chosen accordingly as the inner cube of the module which
 578 surfaces are distant of $4 \times$ scintillator space = 10 cm from the module external surfaces.
 579 The neutrino interactions are simulated using NEUT v5.3.2. The NEUT input neutrino
 580 flux is estimated using JnuBeam v13a and assuming the detector to be located at 1.5°
 581 off-axis, as in Section 5. Note that the event reconstruction efficiency as a function of true
 582 neutrino energy might be changed at 1.5°, due for example to different Q^2 distributions. For
 583 this reason, one has to note that the reconstruction results might slightly be changed from
 584 2.5° and 1.5°. To avoid a similar change on the particle-only reconstruction efficiencies,
 585 they will be presented as a function of variables that completely characterize the particle
 586 kinematic state, *i.e.* its momentum and angle. Figure 33 shows the vertices distributions

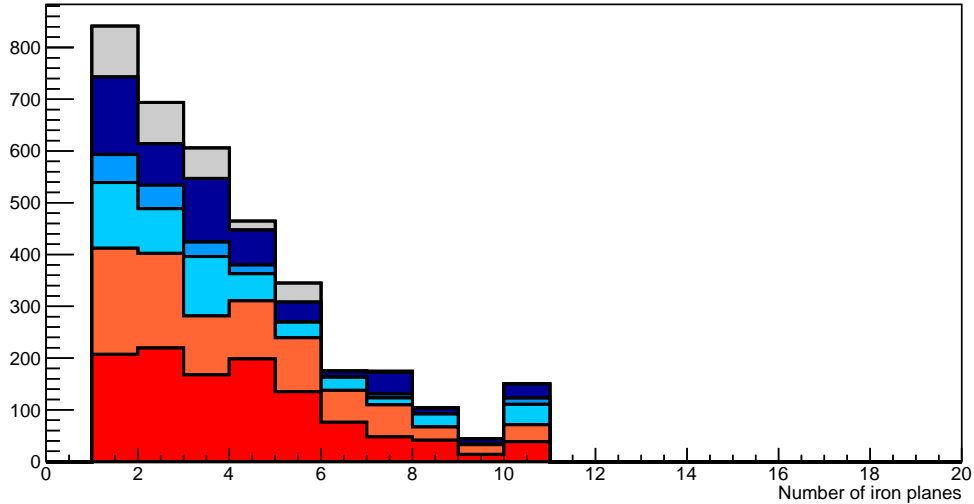


Figure 28: Iron plane numbers in Side-MRD corresponding to the end points of the longest tracks in the selected events in the neutrino-mode.

of the daughter particles of neutrinos interacting one standard WAGASCI water-module.
 In this section, we will show the detector reconstruction and particle identification in this
 phase space, both for leptonic and hadronic particles. We will finally show an empty
 WAGASCI module can highly enhance the ability to constrain the neutrino interaction
 final state which is critical to reduce the corresponding uncertainties.

6.1 Reconstruction algorithm

6.1.1 Description

For this section, an ideal “simulated” reconstruction is developed. A particle is reconstructed if:

- 596 1. The particle is charged.
- 597 2. Lets at least one hit (energy deposit > 2.5 photo-electron) in a scintillator.
- 598
- 599 3. The particle enters one TPC and let one hit in the tracker.

600 Or

601

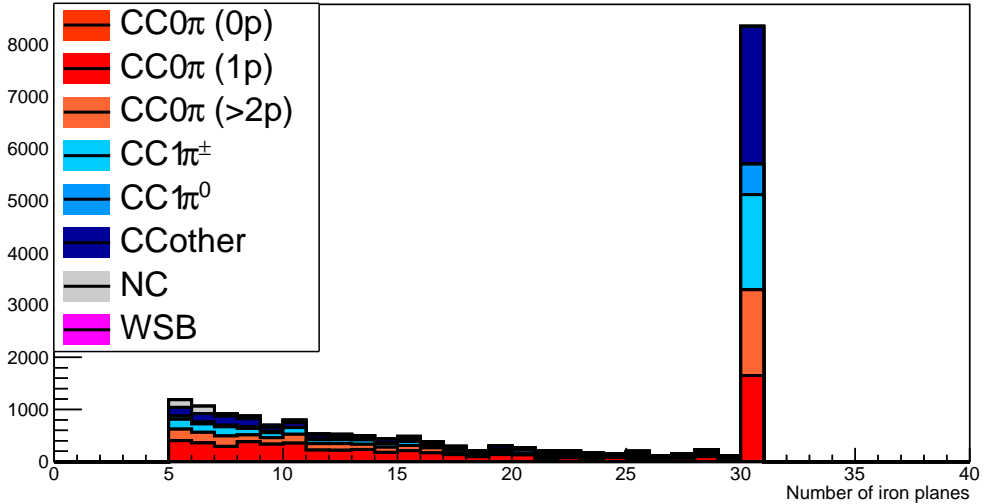


Figure 29: Iron plane numbers in Baby-MIND corresponding to the end points of the longest tracks in the selected events in the neutrino-mode.

- The particle should be long enough to be reconstructed by the detector in at least 2 out of 3 views (XZ, YZ, XY). The length criterion requires the particle to let at least 4 hits in the detector. In the “less favourable case” of pure longitudinal or transverse going tracks, it represents a the track length of $L_{track} \geq 4 \times$ scintillator space = 10.0 cm.
- In the views where particles pass the length criterion, the particle shall not be superimposed with longer tracks in at least two views. The superposition criterion is estimated with the distance inter-tracks (DIT) which corresponds to the orthogonal distance between two tracks at the ending point of the shortest one (see Figure 34). For a track 1, the superposition criterion is tested with every longer tracks that starts at the same vertex. Let \vec{p}_1^a the vector of track 1, and p_1^a its projections in the XZ, YZ and XY planes respectively for $i=1,2,3$. Note that these are projections in a 2D planes and not on a direction vector. In this case, the relative angle between the track 1 and a longer track 2 (of vector \vec{p}_2^a) in a view a is given by:

$$\cos \theta = \frac{\vec{p}_1^a \cdot \vec{p}_2^a}{\|\vec{p}_1^a\| \|\vec{p}_2^a\|} \quad (2)$$

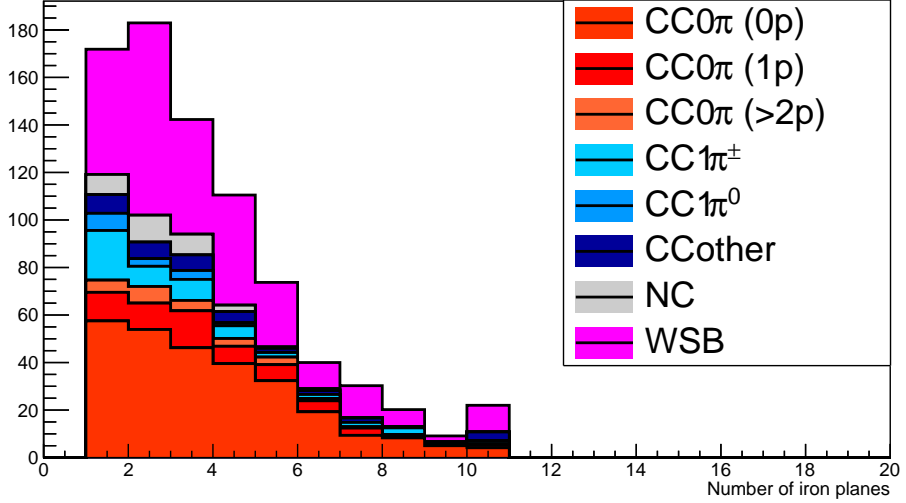


Figure 30: Iron plane numbers in Side-MRD corresponding to the end points of the longest tracks in the selected events in the antineutrino-mode.

and the distance inter track is given by:

$$\text{DIT} = \|\vec{p}_1^a\| \sin \theta \quad (3)$$

The DIT should be higher than $4 \times$ scintillator width for the track 1 to be not superimposed with the track 2 in the view a, which also corresponds to 10.0 cm in the nominal configuration.

6.1.2 Performances

The particle-only reconstruction efficiencies and the reconstruction threshold in momenta are shown in Table 7. This threshold is defined as the maximal momentum for which the reconstruction efficiency is smaller than 30%. The thresholds in muon and pion momenta are 150 MeV/c. Most of the muons are above this threshold (see Figure 33) which leads to a 79% reconstruction efficiency.

The lower pion and proton efficiencies (respectively 52% and 26%) are due to lower efficiencies for similar momenta than muons, coming from strong interactions as shown on Figures 35. Efficiencies of each particle type tend to decrease in the backward region due to particle lower momenta. However, for a fixed momentum value, the reconstruction efficiency is almost uniform which confirms the ability of the WAGASCI detector to reconstruct high angle tracks.

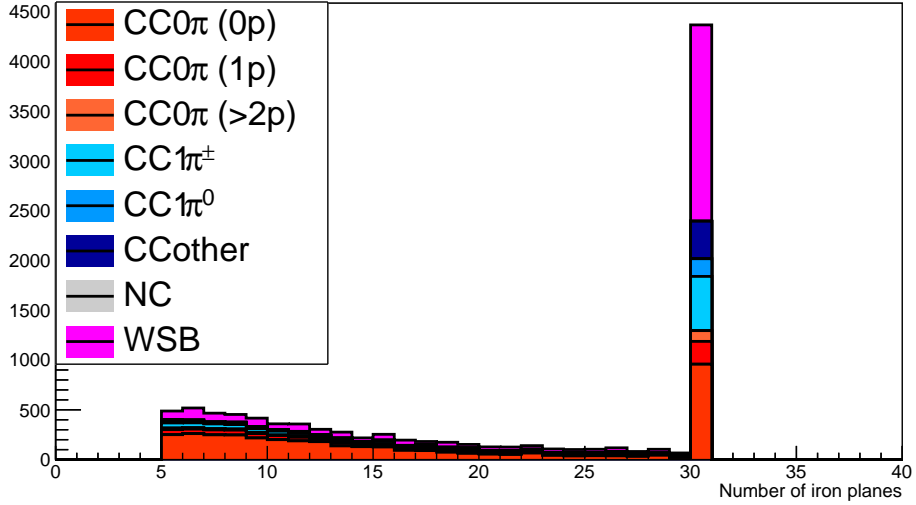


Figure 31: Iron plane numbers in Baby-MIND corresponding to the end points of the longest tracks in the selected events in the antineutrino-mode.

	μ	π	p
Reconstruction Efficiency	79%	52%	26%
Momentum threshold	150 MeV/c	150 MeV/c	550 MeV/c

Table 7: Reconstruction efficiency and momentum threshold for muons, pions and protons. The threshold is defined as the maximal momentum for which particles have a reconstruction efficiency smaller than 30%.

633 The reconstruction is thereafter tested on neutrino events. Table 8 summarizes the
 634 number of reconstructed events and efficiencies for each interaction type. As expected
 635 from the high muon reconstruction efficiency, the charged current interactions have recon-
 636 struction efficiencies $\geq 85\%$.

637 The reconstruction efficiencies as a function of the neutrino energy and muon kinematics
 638 are respectively shown on Figure 36 and 37.

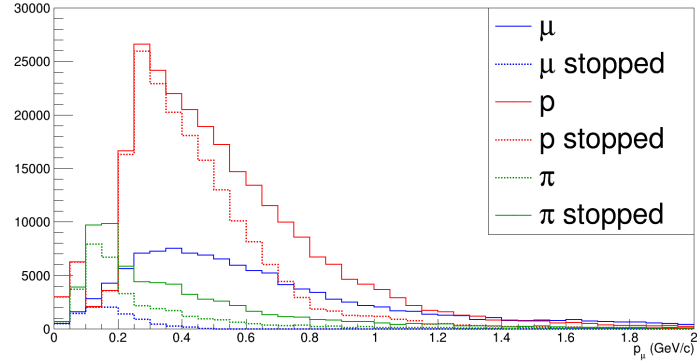


Figure 32: Momentum distribution of true particles in WAGASCI (plain) and corresponding distributions only for particles stopping into the WAGASCI module (dashed).

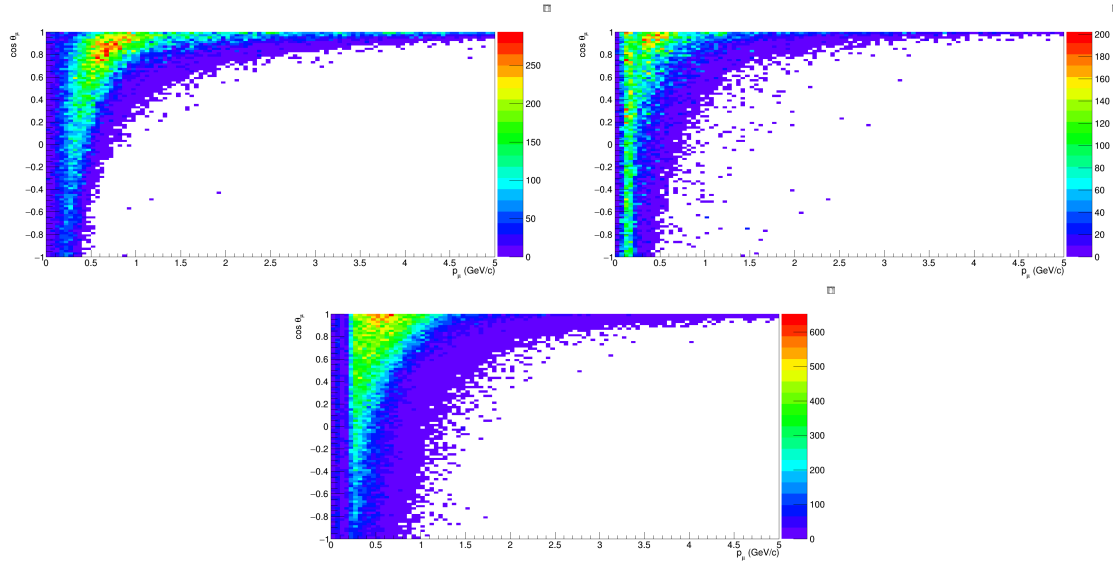


Figure 33: True number of muons (left), charged pions (right) and protons (bottom) in the two WAGASCI water-module as a function of the particles momenta and angles at 1.5° .

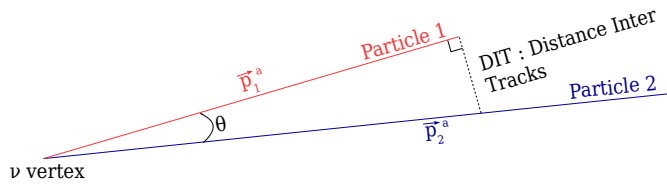


Figure 34: Definition of the distance inter tracks.

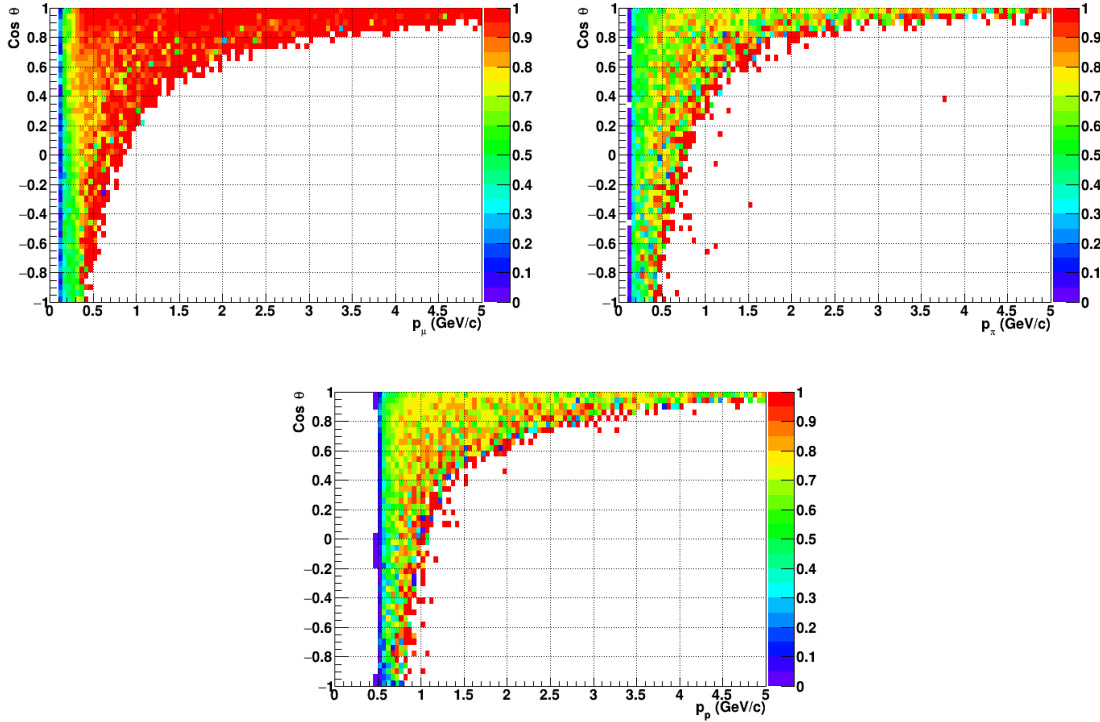


Figure 35: Reconstruction efficiency of muons (left), charged pions (right) and protons (bottom) in the WAGASCI water-module as a function of the particles momenta and angles.

	CC0 π	CC1 π	CCOthers	NC	All
Reconstruction efficiency	85%	87%	91%	22%	68%

Table 8: Number of true interactions reconstructed. The purity and reconstruction efficiency of each true interaction is also shown.

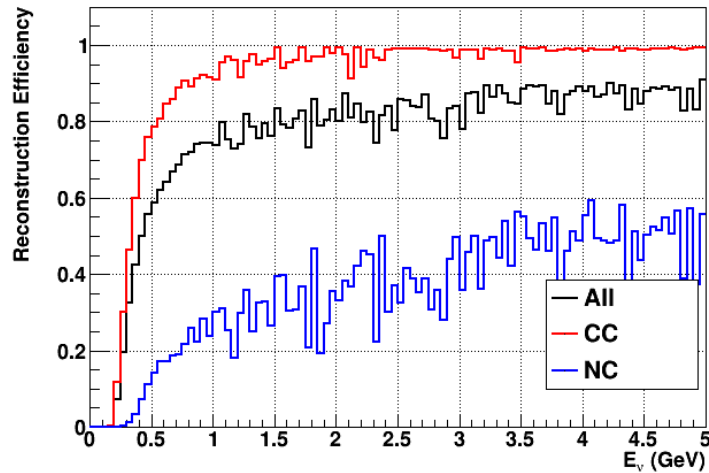


Figure 36: Reconstruction efficiency of all neutrino (black), CC (red) and NC (blue) interactions in the WAGASCI water-module as a function of the neutrino energy.

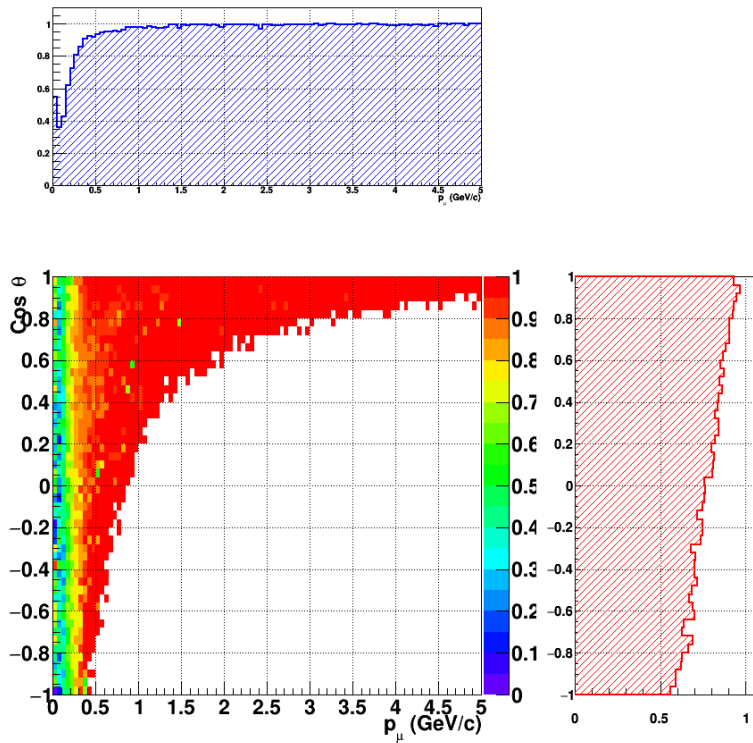


Figure 37: Reconstruction efficiency of CC interactions in the WAGASCI water-module as a function of the muon kinematic variables (momentum and angle).

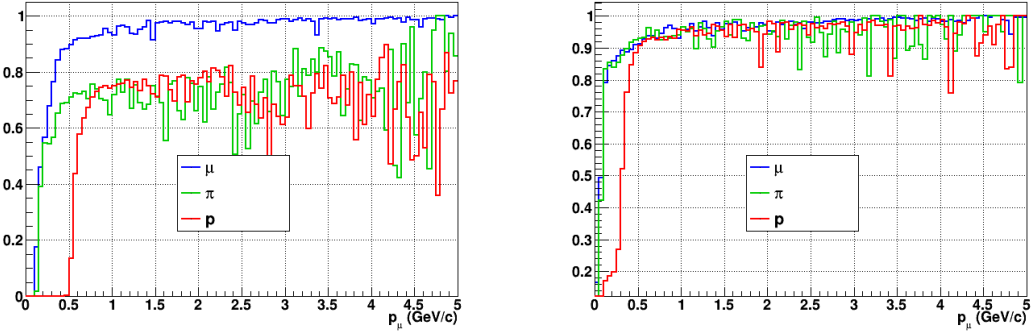


Figure 38: Reconstruction efficiency for muons, pions and protons in the water-in (left) and water-out (right) modules.

639 Note that a Particle Identification Algorithm has been also developed. It is based on
 640 the charge deposition of the particles in the scintillator, of the detection of a decay-electron.
 641 However, this information highly depends on the number of scintillator hit by a particle,
 642 which creates an important difference between a real WAGASCI module and the one used
 643 for the ND280-upgrade simulation. For this reason, the corresponding results will not be
 644 detailed here, but can be found in [?].

645 6.2 Background subtraction: the water-out module

646 In the nominal configuration, 20% of the neutrino interactions occurs on scintillators
 647 (C_8H_8). This background should be removed in order to measure the neutrino interac-
 648 tion on the same target as Super-K, which suppress the differences in cross-section models.
 649 For this purpose, we propose to use a water-out module, where the water is replaced by
 650 air. The detector is therefore fully active and has a 3 mm spatial resolution (scintillator
 651 thickness) which create an ideal detector to reconstruct and identify hadrons, and study
 652 np-nh interactions. The counter-part is the difference in particle energy deposition between
 653 the water and this water-out module that will need to be corrected for. In this section,
 654 we present the capabilities of such a module, and the impact it can have on cross-section
 655 measurements for the neutrino community in general and T2K in particular.
 656 The same reconstruction and selection as the water-in module is applied. Figure 38 shows
 657 the comparison between the water-in and the water-out reconstruction efficiencies for muon,
 658 pions and protons. 90% of the muons and 87% of the pions are reconstructed, while 70%
 659 of the protons are even reconstructed. It allows to lower down the proton threshold to
 660 250 MeV/c (see Table 9).

661 As a consequence of tracking even low momenta particle, the reconstruction efficiency
 662 is uniform and almost maximal on the entire $\cos \theta_\mu$ phase space, as shown on Figure 39.

	μ	π	p
Reconstruction Efficiency Momentum threshold	90% 50 MeV/c	87% 50 MeV/c	70% 250 MeV/c

Table 9: Reconstruction efficiency, proportions of μ -like and non μ -like and momentum threshold for muons, pions and protons in the empty module. The threshold is defined as the maximal momentum for which particles have a reconstruction efficiency smaller than 20%.

663 Since the fiducial mass represents 0.25 tons, the total number of events is divided by a
 664 factor of 3 compared to the water-in module. The water-out module offers interesting
 665 possibilities to study np-nh interaction since 70% of the protons are reconstructed. In the
 666 future, a possible separation as a function of the number of proton track will be studied.
 667 Moreover, we are currently pursuing the use of single and double transverse variables (cite
 668 Xianguo) to open new possibilities for separating np-nh from Final State Interactions, or
 669 for isolating the interactions on hydrogen from interactions on carbon in this module.

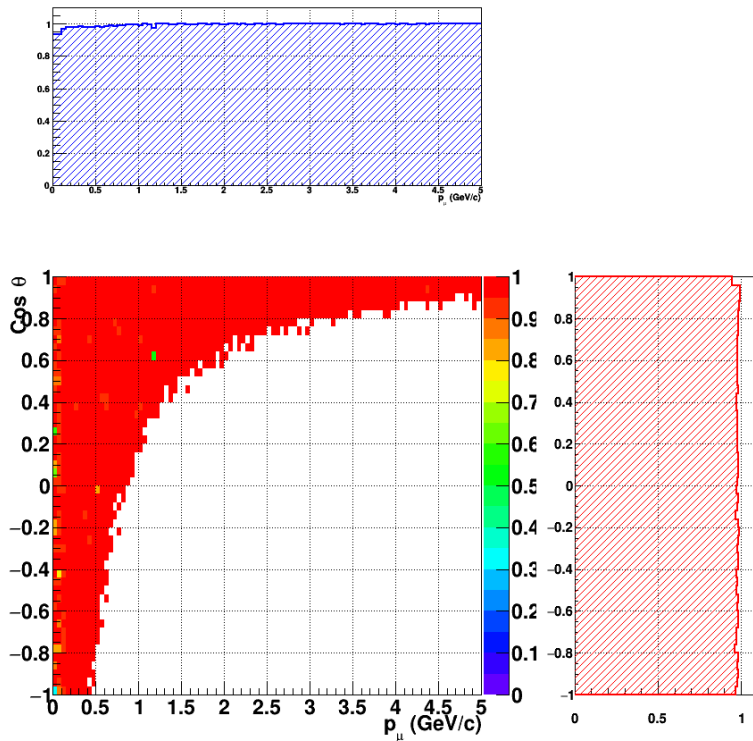


Figure 39: Reconstruction efficiency of CC interactions in the WAGASCI empty module as a function of the muon kinematic variables (momentum and angle).

670 **7 Schedule**

671 We would like to start a physics data taking from T2K beam time after the summer
672 shutdown in 2018. By then, commissioning and tests of the detectors will be completed
673 in J-PARC T59. The experiment can run parasitically with T2K, therefore we request no
674 dedicated beam time nor beam condition as discussed in the following section.

675 Once the approved POT is accumulated, the WAGASCI modules will be removed
676 from the experimental site, but we would like to keep the Baby-MIND and the Side-MRD
677 modules on the B2 floor of the NM pit as common platforms of future neutrino experiments
678 using the T2K neutrino beam.

679 **8 Requests**

680 **8.1 Neutrino beam**

681 The experiment can run parasitically with T2K, therefore we request no dedicated beam
682 time nor beam condition. As data taking periods, we request the ‘nominal’ T2K one-year
683 operation both for the neutrino beam and the antineutrino beam. The T2K has been
684 requesting 0.9×10^{21} POT/year and actually accumulating about 0.7×10^{21} POT/year in
685 recent years. For each year, starting from the Autumn, T2K is running predominantly in
686 the neutrino mode or in the antineutrino mode. Our request is to have one-year neutrino-
687 mode data and another one-year antineutrino mode data assuming that the POT for the
688 fast extraction in each year is more than 0.5×10^{21} POT.

689 **8.2 Equipment request including power line**

690 We request the followings in terms of equipment on the B2 floor:

- 691 • Site for the WAGASCI modules, Side-MRD modules and BabyMIND and their elec-
692 tronics system on the B2 floor of the near detector hall (Fig. 3).
- 693 • Anchor points (holes) on the B2 floor to secure the WAGASCI modules, Side-MRD
694 module and Baby-MIND (Fig. ??)
- 695 • Power line for the magnets in Baby-MIND: 400 V tri-phase 48-to-62 Hz, capable of
696 delivering 12 kW.
- 697 • Electricity for electronics and water circulation system, 3 kW, standard Japanese
698 electrical sockets.
 - 699 1. Online PCs: 2.1 kW
 - 700 2. Electronics: 0.7 kW
 - 701 3. Water sensors: ?

- 702 • Air conditioner for cooling heat generation at Baby-MIND magnets, online PCs and
703 electronics
- 704 • Beam timing signal and spill information
- 705 • Network connection

706 **8.2.1 Baby MIND Equipment request including power line**

707 We request the following in terms of equipment on the B2 floor:

- 708 • Site for the Baby MIND detector and its electronics systems on the B2 floor of the
709 near detector hall.
- 710 • Anchor points (holes) on the B2 floor to secure the 9 support frames, of order 4 holes
711 per frame, detailed floor plans to be communicated in a separate document.
- 712 • Power line for the magnet: 400 V tri-phase 48-to-62 Hz, capable of delivering 12
713 kW. We have a wish for the magnet power line to be installed and available to us by
714 beginning of March 2018.
- 715 • Electricity for electronics, 1 kW, standard Japanese electrical sockets.
- 716 • Beam timing signal and spill information
- 717 • Network connection

718 The infrastructure for much of the above exists already, and will be shared in part with
719 the WAGASCI experiment. Exceptions are the power line for the magnet and holes in the
720 B2 floor to anchor the detector support structures.

721 **9 Conclusion**

722 **References**

- 723 [1] K. Abe et al. Measurement of the muon neutrino inclusive charged-current cross
724 section in the energy range of 13 GeV with the T2K INGRID detector. *Phys. Rev.*,
725 D93(7):072002, 2016.
- 726 [2] M. Antonova et al. Baby MIND Experiment Construction Status. In *Prospects in*
727 *Neutrino Physics (NuPhys2016) London, London, United Kingdom, December 12-14,*
728 2016, 2017.
- 729 [3] K. Nitta et al. The k2k scibar detector. *Nucl. Instrum. Meth. A*, 535:147, 2004.

- 730 [4] K. Abe et al. (T2K Collaboration). Measurement of the inclusive ν_μ charged current
731 cross section on iron and hydrocarbon in the t2k on-axis neutrino beam. *Phys. Rev.*
732 *D*, 90:052010, 2014.
- 733 [5] F. Magniette F. Gastaldi, R. Cornat and V. Boudry. A scalable gigabit data acquisition
734 system for calorimeters for linear collider. *proceedings of TIPP2014*, page PoS 193,
735 2014.
- 736 [6] J. Fleury, S. Callier, C. de La Taille, N. Seguin, D. Thienpont, F. Dulucq, S. Ahmad,
737 and G. Martin. Petiroc and Citiroc: front-end ASICs for SiPM read-out and ToF
738 applications. *JINST*, 9:C01049, 2014.
- 739 [7] M. B. Barbaro J. A. Caballero T. W. Donnelly G. D. Megias, J. E. Amaro. Inclusive
740 electron scattering within the susav2 meson-exchange current approach. *Phys. Rev.*
741 *D*, 94:013012, 2016.
- 742 [8] M. Valverde J. Nieves, J. E. Amaro. Inclusive quasi-elastic neutrino reactions. *Phys.*
743 *Rev. C*, 70:055503, 2004.
- 744 [9] Yu. G. Kudenko, L. S. Littenberg, V. A. Mayatsky, O. V. Mineev, and N. V. Ershov.
745 Extruded plastic counters with WLS fiber readout. *Nucl. Instrum. Meth.*, A469:340–
746 346, 2001.
- 747 [10] O. Mineev, Yu. Kudenko, Yu. Musienko, I. Polyansky, and N. Yershov. Scintillator
748 detectors with long WLS fibers and multi-pixel photodiodes. *JINST*, 6:P12004, 2011.
- 749 [11] Etam Noah et al. Readout scheme for the Baby-MIND detector. *PoS*, Photo-
750 Det2015:031, 2016.
- 751 [12] Omega. Spiroc 2 user guide. 2009.